Journal of Materials Chemistry C

ROYAL SOCIETY OF CHEMISTRY

REVIEW

View Article Online
View Journal | View Issue

Cite this: J. Mater. Chem. C, 2024, 12, 4544

Unlocking the potential of perovskite-based nanomaterials for revolutionary smartphone-based sensor applications

Dan Li, *[a] Pengfei Zhuang [a] and Cai Sun*[b]

Received 8th December 2023,
Accepted 27th February 2024

DOI: 10.1039/d3tc04505f

rsc.li/materials-c

The increasing expense and complexity of conventional physical exams may lead to delayed disease diagnoses, creating substantial difficulties for many patients. In response, smartphone-based sensing technologies have emerged, offering a promising solution to make health diagnostics more accessible. Perovskite-based nanomaterials stand out with their adaptable structure, making them an important player in sensor enhancement due to their wide-ranging sensing capabilities and excellent physicochemical characteristics. While perovskites demonstrate advantageous optoelectronic properties, fortifying their stability is a crucial aspect that continues to be a central theme in current research and development endeavors. This article examines the advancement of smartphone-based sensors *via* the incorporation of Perovskite-based nanomaterials and suggests strategies for further optimizing their characteristics. It provides a detailed overview of their applications in different smartphone sensing areas, including but not limited to optical and photothermal-pyroelectric methods. Our in-depth analysis highlights the crucial role of Perovskite-based nanomaterials in the development of devices and the complexity of sensor manufacturing. We also explore their potential in seamlessly integrating with wearable devices connected to smartphones, thus streamlining the diagnosis process. Moreover, we anticipate their revolutionary impact in advancing smartphone sensors. This combination is poised to establish a more accessible and unified method for health monitoring.

1. Introduction

Smartphones, integral to modern lifestyles, have evolved significantly, becoming essential tools in a variety of applications, including health diagnostics.[1] The rapid advancements in mobile technology have not only refined the embedded hardware and software but also enriched these devices with a variety of sensors, each serving distinct functions in health-related applications.[2,3] Prominent among these sensors are high-resolution cameras, which offer imaging capabilities crucial for telemedicine and skin condition monitoring.[4] Accelerometers and gyroscopes provide vital data on physical movement and orientation, useful in tracking physical activity and detecting falls. Temperature sensors play a pivotal role in environmental monitoring, potentially offering insights into body temperature fluctuations. Light sensors, primarily used for screen brightness adjustment, can also be repurposed for monitoring sleep patterns or detecting changes in ambient light conditions related to health.[5]

The efficacy of these sensors in health diagnostics is significantly enhanced by the incorporation of materials with specific physical and chemical properties. These materials are carefully selected for their biocompatibility, ensuring safe interaction with human physiology. Chemical stability is another crucial attribute, as it guarantees consistent performance under various conditions. Sensitivity is paramount, particularly in detecting minute physiological changes or biomarkers, which is essential for early disease detection and monitoring. Additionally, smartphones can feature USB interfaces for data transfer and connectivity, Bluetooth for wireless communication, and an array of other sensors.[6] These include pressure sensors, useful in altimetry and potentially in blood pressure monitoring; thermal imaging sensors, which could play a role in fever detection; and sensors for distance, gravity, and direction, offering broader applications in fitness and navigation.[7–9] The latest research in this field predominantly revolves around enhancing optical and biochemical sensors, refining motion detectors, and improving environmental sensors.[10–12]

The fusion of sensor innovation with smartphone technology may bring a pivotal shift in the landscape of point-of-care diagnostics, signaling a future where comprehensive health monitoring is seamlessly integrated into the fabric of everyday life.[5,13–16] The success of these sophisticated sensors is

[a] College of Pharmacy, Jinzhou Medical University, 40, Songpo Road, Linghe District, Jinzhou, China. E-mail: danli@jzmu.edu.cn
[b] AECC Shenyang Liming Aero-Engine, 149, South Sijing Street, Heping District, Shenyang, China. E-mail: suncai2010@126.com

fundamentally dependent on the innovative materials from which they are constructed.[17–19] A variety of nanomaterials have demonstrated potential in this arena: graphene, with its extraordinary electrical conductivity and surface area;[20–22] gold-based nanomaterials,[23–26] revered for their distinctive plasmonic properties; and polymer dots,[27,28] quantum dots,[29,30] which may integrate seamlessly with existing semiconductor frameworks. Yet, within this innovative spectrum, Perovskite-based nanomaterials offer unmatched benefits for the evolution of smartphone-integrated sensors. Perovskite materials, characterized by the general formula ABX_3, allow for a customizable composition-'A' and 'B' as varying cations, often metallic or organic, and 'X' as an anion, typically a halide.[31] ABX_3 structure, encompasses a wide range of variations beyond this basic formula. For instance, double perovskites (A_2BBX_6) feature two different B-site cations, offering unique magnetic and electronic properties.[32] Layered perovskites, exemplified by $A_{n+1}B_nX_{3n+1}$ (Ruddlesden–Popper phase) and $A_{n-1}B_nX_{3n+1}$ (Dion–Jacobson phase), feature multiple perovskite layers interspersed with either double (in Ruddlesden–Popper) or single (in Dion–Jacobson) layers of A-site cations. This structural variation significantly impacts their electronic properties, making them particularly valuable in the field of photovoltaics.[33–35] For example, some Ruddlesden–Popper phases, characterized by their ABX_4 structure, showcase a unique composition of alternating perovskite and rock-salt layers. This distinctive structure broadens the material's utility across numerous technological fields, particularly in the development of optoelectronic devices with lower energy consumption.[36–38] Hybrid perovskites blend organic and inorganic elements, allowing for enhanced tunability and processing ease.[39] Their physical properties, including a small open-circuit voltage deficit and high-power conversion efficiency, are particularly beneficial for Solar energy conversion, with the aim of reducing the levelized cost of electricity.[40–42] Doped perovskites, achieved by substituting ions at A, B, or X sites, enable tailored properties and structures.[43] This structural flexibility enables precise tailoring of optical and electric properties, setting the stage for a vast range of sensing applications beyond just fluorescent and electrochemical sensing.[44–46]

Perovskite-based nanomaterials demonstrate a diverse range of functionalities in advanced sensing technologies, encompassing areas like optical sensing, mechanochemical detection, piezoelectric responses, thermal sensing, and integrated modalities such as photothermal-pyroelectric sensing.[47–49] Their integration into smartphone-based sensors may be significantly enhanced by their superior luminescence properties and the ability to precisely tailor their emission spectra.[50–53] This attribute is critically advantageous for incorporation into smartphone platforms, where inherent optical limitations of the devices can be effectively compensated by the remarkable brightness and tunable emission properties.[54]

The high surface-to-volume ratio and rapid electron transfer capabilities inherent to Perovskite-based nanomaterials are fundamental for the efficient transduction of biological interactions into electrical signals.[55–57] This characteristic substantially enhances the performance of smartphone-based sensors in providing immediate and accurate biological analysis. Additionally, the lattice structure is notably malleable, allowing for intricate material-level engineering.[58–60] This also affords the creation of highly specific binding sites for targeted analytes, achieving a level of specificity that transcends traditional surface-level modifications.[61–64]

Furthermore, the synthesis of perovskite-based nanomaterials is both scalable and economically viable, rendering them an attractive proposition for the mass production of sophisticated biosensors.[65–67] When combined with the widespread accessibility and functionality of smartphones as detection platforms, perovskite-based nanomaterials may offer a cost-effective and widely applicable solution for continuous health monitoring and diagnostics in a variety of healthcare settings. They also demonstrate changes in electrical resistance in response to environmental variations, offering robust and reliable biosensing capabilities. This feature is particularly crucial for the monitoring of metabolic or enzymatic reactions through smartphone interfaces.[68–70] The inherent stability of Perovskite-based nanomaterials ensures their longevity and reduces maintenance demands.[71–73]

In the realm of peer-reviewed research, perovskite-based sensors are gaining attention for their impressive potential in smartphone applications, despite being in an embryonic stage. Existing literature has delved into the functional mechanisms and sensing capabilities, and various devices employing perovskites. Zhang *et al.*, for instance, have provided a comprehensive overview of the functionalities of micro-nano structures in optoelectronics, highlighting their role in enhancing light trapping, modulation, carrier dynamics, and mechanical robustness.[74] These advancements have implications for technologies such as solar cells, LEDs, photodetectors, and lasers. Zhou *et al.* have taken a holistic approach, linking critical elements of perovskite research, ranging from characterization techniques and structural variations to properties and device performance.[75] They particularly emphasized the influence of microstructures on the photophysical properties of perovskites and how these affect the degradation and efficacy of perovskite solar cells. He *et al.* have focused on perovskite oxide-based non-enzymatic electrochemical sensors, exploring the latest in electrochemical detection methods, doping strategies, and ways to enhance performance.[76] Additionally, Yang *et al.* have shed light on the instability issues in perovskite LEDs, analyzing the impact of heat, moisture, light, and ion migration.[77] While research on perovskites in smartphone-based sensor technology is not covered in literature, we aim to thoroughly analyze the role of perovskite nanocrystals (PNCs) in the burgeoning field of smartphone-enabled sensors. Our focus is on the unique characteristics of PNCs and their role in enhancing the functionality of various applications as reported in existing literature, including optical (OP), photo-thermal-pyroelectric (PT-PE), and wearable sensors (refer to Fig. 1). Additionally, this exploration delves into the prospects of utilizing these materials in health diagnostics through wearable technology linked to smartphones. This investigation into an emerging field emphasizes the critical role of PNCs in bridging the gap between laboratory-level diagnostic

Fig. 1 Common uses of PNCs in smartphone-integrated sensors encompass photothermal-Pyroelectric applications, optical sensing technologies, and advancements toward integration in wearable diagnostic devices.

accuracy and the ease of smartphone usage, signifying a breakthrough in the realm of digital health monitoring.

2. Optical sensors

The pivotal role of perovskite-based materials in the development of optical sensors for smartphone applications may underscore a transformative stride in analytical technology. One of the reasons for the selection of perovskites is primarily due to their remarkable enzyme-like catalytic activities. This property allows perovskite materials to act as pseudo-enzymes, catalyzing reactions that lead to detectable changes, similar to natural enzyme-substrate interactions. Furthermore, perovskites are renowned for their exceptional photoluminescence (or fluorescence) and electroluminescence (ECL) traits. These photophysical properties are crucial in enhancing the sensor's ability to detect and quantify various analytes with high precision, as they allow for the measurement of light emission changes upon interaction with different analytes. This sensitivity to light and color changes translates into a more accurate detection and quantification of substances. By combining these advanced sensors with the computational prowess of smartphones, there is a possibility of revolutionizing sectors like environmental monitoring, healthcare diagnostics, and biochemical analysis.

2.1. Enzyme-like activity

Perovskite-based nanomaterials have demonstrated remarkable enzyme-like functions, positioning them as versatile nanozymes.[78] As detailed in Table 1, these perovskite nanozymes encompass a spectrum of biochemical processes, including activities similar to peroxidase (POD), catalase (CAT), superoxide dismutase (SOD), and oxidase (OXD). For instance, PM-$CsPbX_3$ NCs exhibit POD-like activity and are noteworthy for their self-reporting substrate detection capabilities, which negate the need for additional chromogenic substrates.[79] This property is particularly advantageous in the development of multi-color bioinks and metabolite-responsive paper analytical devices, broadening the scope of their applicability in various bioanalytical fields. Similarly, $CsPbBr_3$ NCs, also displaying POD-like activity, stand out for their dual-signal generation ability, producing both fluorescent and colorimetric signals.[80] Their enhanced aqueous stability, afforded by a lipid shell, along with antifouling properties and chemical flexibility for molecular conjugation, contribute to more precise bioassays. These characteristics make them ideal for a dual-readout immunoassay in detecting prostate specific antigen (PSA). Moreover, $LaFeO_3$ microspheres (Ms), with superior POD-like catalytic activity due to its mesoporous structure, show high reproducibility and stability in colorimetric sensing.[81] Their excellent anti-interference capability in real sample analysis, coupled with convenience, stability, and low cost, make them suitable for out-of-lab use, such as in a colorimetric detection system for glycyrrhizin acid (GA). $LaNiO_3$ nanocubes further exemplify the potential of perovskite nanozymes in colorimetric biosensing.[82] Their increased POD-like activity, enhanced by oxidation state and porous structures, enables them to perform facile colorimetric assays for H_2O_2, glucose, and sarcosine, demonstrating their versatility in practical applications. Additionally, the unique composition of $SrCoO_3/Co_3O_4$ Ns enhances

Table 1 Advantages and applications of typical perovskites demonstrating enzyme-like activities

Perovskites	Nanozymes	Advantages	Potential applications	Ref.
PM-$CsPbX_3$ NCs	POD	Self-reporting substrate detection; no need for additional chromogenic substrates	Multi-color bioinks and metabolite-responsive paper analytical devices	79
$CsPbBr_3$ NCs	POD	Dual-signal generation; Enhanced aqueous stability with lipid shell; Antifouling properties reducing biological impurities; chemical flexibility for molecular conjugation; more precise bioassays due to dual-signal readout	A dual-readout immunoassay for detecting PSA	80
$LaFeO_3$ Ms	POD	Superior POD-like catalytic activity due to mesoporous structure; High reproducibility and stability in colorimetric sensing; excellent anti-interference capability in real sample analysis; convenience, stability, and low cost make it suitable for out-of-lab use	A colorimetric detection system for selective and sensitive identification of GA	81
$LaNiO_3$ nanocubes	POD	Increased POD-like activity from oxidation state; enhanced activity *via* porous structures; POD activity 58-fold over Ni^{2+} NiO, 22-fold over Ni^0 NPs, 2-fold greater activity than $LaNiO_3$ NPs.	Facile colorimetric assays for H_2O_2, glucose, and sarcosine	82
$SrCoO_3$/Co_3O_4 Ns	POD	$SrCoO_3$/CQDs enhance SOD/electron–hole production, accelerating electron transfer; catalytic activity greatly increased with $SrCoO_3$/CQDs; tigecycline binds to CQDs@$SrCoO_3$/Co_3O_4, enhancing catalytic efficiency.	Molecularly imprinted colorimetric sensor for TGC	83
TMO-e_g occupancy	POD	$LaNiO_{3-\delta}$ identified as the most catalytically active among over 20 POD-like nanozymes tested	Encouragement for application of TMO-e_g occupancy	87
$LaMnO_{3+\delta}$	OXD	Simple preparation *via* electrospinning and calcination; superior OXD activity due to effective composition and morphology	Dispersion or monolithic form for on-demand sensing	88
Strontium oxides	POD	High sensitivity and convenience in bisphenol detection; utilizes strontium oxide for enhanced sensing capability	Identifying mixed bisphenol ratios and classifying real samples	89
Au-$LaNiO_{3-\delta}$ NFs	OXD	2.38-fold increase in OXD activity due to carboxyl group; 5.27-fold enhancement in SERS activity from carboxyl group addition; enhanced oxidation *via* O–O species production from oxygen interaction.	Constructing nanozyme-linked immunosorbent assays for cancer diagnosis	90

PM, phospholipid membranes; Ms, microspheres; GA, gallic acid; Ns, nanospheres; TGC, tigecycline; CQDs, carbon quantum dots; TMO-e_g occupancy, TMOs-based nanozymes with their e_g occupancy. TMOs, transition metal oxides; $LaNiO_{3-\delta}$, an example of TMOs covering e_g occupancies of 0–2; BiOS, $Bi_{10}O_6S_9$ nanosheet arrays; strontium oxide, $SrMnO_3$, $SrRuO_3$ and $SrFeO_3$; NFs, nanofibers.

SOD/electron–hole production, accelerating electron transfer.[83] This catalytic activity is significantly increased with $SrCoO_3$/carbon quantum dots (CQDs), illustrating the potential of perovskite nanozymes in constructing molecularly imprinted colorimetric sensors, such as those for tigecycline (TGC).

In the pursuit of advanced biosensing technologies, Feng *et al.* have employed perovskite nanozymes to create a sensitive and specific colorimetric assay for the detection of nuclear matrix protein 22 (NMP22), a clinical biomarker for bladder cancer.[84] They discovered that halide ions, introduced *via* a straightforward anion exchange, can modulate the catalytic performance of these nanozymes. Remarkably, $CsPbI_3$ nanocrystals demonstrated a 24-fold enhancement in catalytic efficiency compared to their $CsPbBr_3$ counterparts. Such improvements in catalysis translated to a colorimetric immunoassay that achieved a detection limit as low as 0.03 U mL^{-1}, surpassing traditional assays in performance. Moreover, a $CsPbI_3$ NCs@PL-based immunoassay was devised, with a visual signal enhancement achieved *via* the attachment of biotin-labeled detection antibodies to the target molecules, as illustrated in Fig. 2a. Quantitative analysis through absorbance measurements confirmed a broad detection range and excellent selectivity for NMP22, outperforming other halide-incorporated nanozyme-based assays, as evidenced in Fig. 2b and c. The assay's precision was affirmed through the absence of signal interference from common urinary substances (Fig. 2d) and validated with real patient samples (Fig. 2e). Building on these phenomena, a competitive smartphone-based sensing method over conventional colorimetric assays through the application of $CsPbI_3$ may be achieved. While this work highlights the effectiveness of the $CsPbI_3$ NCs@PL-based immunoassay in detecting bladder cancer biomarkers, it lacks crucial details on integrating this technology with smartphone sensors and ensuring the device's portability. This platform may involve the use of smartphone cameras for high-resolution image capture of the assay results. These elements may be vital for the technology's practical application in real-world scenarios.

Jiang *et al.*'s research advanced the field by creating nanoparticles (NPs) on perovskite oxides through *in situ* exsolution. This process was driven by A-site defects under a reducing atmosphere, effectively enhancing POD-like activity. Using $La_{0.9}B_{0.9}B'_{0.1}O_{3-\delta}$ (LMIO, with B as Mn/Fe and B′ as Ir/Ru), $La_{0.9}Mn_{0.9}Ru_{0.1}O_{3-\delta}$ (LMRO), $La_{0.9}Fe_{0.9}Ir_{0.1}O_{3-\delta}$ (LFIO), and $La_{0.9}Fe_{0.9}Ru_{0.1}O_{3-\delta}$ (LFRO) as base materials, Ir or Ru NPs were exsolved on their surfaces. Among these, Ir/LMIO exhibited the highest POD-like activity and was utilized to develop a bioanalytical platform for detecting alkaline phosphatase (ALP), offering a broad detection range and low detection limit (Fig. 2g).[85] Adapting this system for use with a smartphone-based platform could greatly improve its convenience and reach, making routine bladder cancer screening more accessible. Utilizing a smartphone for this purpose would also allow for easy capturing of images and color detection, leveraging the smartphone's camera for prospective analysis.

Ye *et al.* advanced the application of perovskite nanozymes by incorporating them into a smartphone-based biosensing

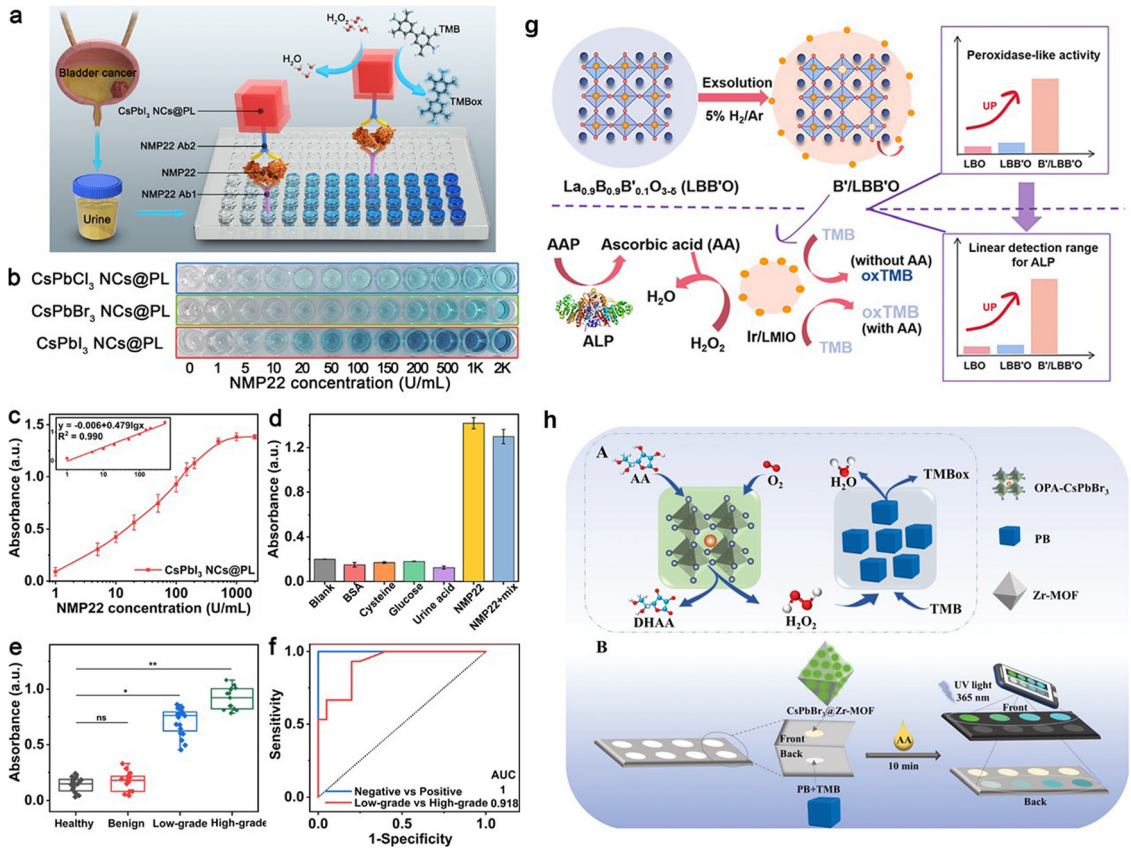

Fig. 2 Evaluation of NMP_{22} using $CsPbI_3$ NCs@PL-Enhanced ELISA: (a) Schematic of enhanced ELISA. (b) NMP_{22} standard detection visualized with $CsPbX_3$ NCs@PL-ELISA. (c) Absorbance for varying NMP_{22} concentrations (0–2000 U mL^{-1}) using $CsPbI_3$ NCs@PL-ELISA. (d) Selectivity test for different interferences. (e) Urine sample absorbance from healthy individuals (n = 20), benign cystitis cases (n = 15), and low- to high-grade patients (n = 35). (f) ROC curves for urine samples; AUC is 1 for healthy *vs.* patient (*P < 0.05), 0.918 for low- *vs.* high-grade (*P < 0.05). Adapted with permission.[84] Copyright 2023, American Chemical Society. (g) Synthesis schematic for noble-metal NPs on perovskite *in situ* exsolution and the subsequent colorimetric assay for ALP activity. Adapted with permission.[85] Copyright 2021, American Chemical Society. (h) Proposed biomimetic cascade catalysis pathways with OPA-$CsPbBr_3$ NCs and PB (A); dual-mode ratiometric fluorescence and colorimetric detection of AA in paper-based devices (B). Adapted with permission.[86] Copyright 2023, Wiley-VCH.

system for neurochemical analysis of ascorbic acid (AA) (Fig. 2h).[86] This platform, employing octylamine-modified polyacrylic acid capped $CsPbBr_3$ NCs, not only reached remarkable detection thresholds but also demonstrated the feasibility of transitioning from lab-centric diagnostics to portable, point-of-care testing. The union of their high catalytic proficiency, adjustable activity, and compatibility with smartphone-based optical sensing platforms signals a transformative development in point-of-care diagnostics.

2.2. Bright fluorescence

In the field of fluorescence-based detection, perovskite-based nanomaterials exhibit unparalleled photoluminescence quantum yields (PLQY), surpassing many existing fluorescent substances used in sensor technology, as shown in Table 2. Specifically, some organometal halide perovskites with PLQYs approaching 100% offer significant benefits for the advancement of ultra-sensitive biosensors coupled with smartphone technology.[91] Their unique crystal structures and strong light-matter interactions contribute to their high PLQY, exemplified by methylammonium lead iodide ($CH_3NH_3PbI_3$) perovskites, which exhibit near-unity quantum yield under optimal conditions.[92] This high PLQY, alongside the capacity to fine-tune emission across a spectrum, positions perovskites as superior materials for smartphone-based sensor applications.[93–95]

The application of perovskites in detecting UV light with silicon (Si) detectors in smartphone cameras is particularly promising. $CsPbBr_3$ PNCs have been discovered to possess exceptional down-converting properties, which expand the Si detectors' sensitivity to UV light. This has been capitalized upon by Tian *et al.*, who have applied a perovskite QD color-converting layer to the camera lenses of smartphones, leading to the invention of novel sensors.[96] These include a UV radiation sensor and a water chemical oxygen demand (COD) sensor, both utilizing smartphone apps for efficient measurement, as demonstrated in Fig. 3(I)a and b. The conversion of UV light to visible light by perovskite QDs is not only rapid but also offers a higher PLQY than other materials, which is advantageous for both UV-light communication and sensing applications.

The inherent instability of $CsPbX_3$ perovskite QDs in the presence of water, light, and heat presents challenges for their

Table 2 Overview of high-fluorescence Perovskites: characteristics and strategies for enhancing fluorescence

Materials	Strategy	Excitation/ Emission	Quantum yield/efficiency	Potential application	Ref.
$CH_3NH_3PbI_3$ film	Reduce non-radiative recombination	532 nm/700–840 nm	Internal QE: 91.9 ± 2.7%	High-open-circuit-voltage devices	100
$CsPbBr_xCl_{3-x}$ QDs	Passivate the surface Cl vacancy defects	365 nm/460 nm	QY: 89%	Promoting the balanced development of the three primary colors	101
$CsPbX_3$ QDs	Solvent-polarity-engineered controllable synthesis	365 nm/410–700 nm	QY: 72%	Optoelectronic applications	102
$CsPbI_3$	TOP surface passivation	365/673–692 nm	QY: ~100%	Both QD-based light-harvesting and -emitting devices	103
$CsPbX_3$(X = Cl, Br, I)	Supersaturated recrystallization	365 nm/513 nm	QY: up to 95%	Optoelectronic devices, as well as sensors and memristors	104
PA_6InCl_9-Sb (2.5%Sb^{3+})	Doping Sb^{3+} into PA_6InCl_9	282 nm/White	QY: ~100%	White LEDs, UV light detectors, and advanced anti-counterfeiting technologies	105
$CsPbBr_xI_{1-x}$	Control halide composition and thickness	400 nm/530 nm	QY: up to 75-92%	Not mentioned	106
photopolymerizable $CsPbX_3$ (X = Cl, Br, I)	Covalent integration of photopolymerizable PQDs with a 4D-printed shape-morphing LCE	365 nm/400–700 nm	QY: 60–90%	Printable, wearable, and intelligent photonics and optoelectronics	107
$CsCdCl_3$:Mn^{2+}	Mn^{2+} doping increases the optical absorption edge band of $CsCdCl_3$	254 nm/585 nm	QY: 91.4%	PL imaging agents and anti-counterfeiting materials.	108
$CsPbI_{3-x}Br_x$ NCs	KBr doping with quaternary ammoniums prevented halide segregation and maximized passivation of surface defects	365 nm/636 nm	QY: 88%–100%	Optoelectronic applications that demand a constant band gap	109
$CsPbX_3$@PVDF-HFP/PS	PFS-assisted electrospinning technology	451.5–650.8 nm	QY: 90%	Fluorescence detection	110

TOP, trioctylphosphine; PQDs, perovskite quantum dots; LCE, liquid crystal elastomer; PVDF-HFP, Poly vinylidene fluoride-*co*-hexafluoropropylene; PS, polystyrene

direct application in fluorescence sensing. Encapsulation within metal–organic frameworks (MOFs) has proven to improve stability and functional versatility, broadening the scope of perovskite QDs in various applications. Shang *et al.* have leveraged this enhanced stability by integrating single drop microextraction (SDME) with smartphone-based detection systems, which refines the monitoring of catalytic degradation processes.[97] The perovskite QDs, incorporated into MOF-5 structures, act as colorimetric sensors, and the smartphone's analytical capabilities are harnessed to compute B/G values for precise and immediate *in-situ* reaction monitoring, as outlined in Fig. 3(II)a–f. Advancements in perovskite nanocrystal applications in biosensing have been furthered by Wang *et al.*, who developed a dual-readout lateral flow immunoassay (LFIA) strip for carcinoembryonic antigen (CEA) detection using $CsPbBr_3$ NCs.[98] These NCs, bound with an amphiphilic polymer ligand, display strong fluorescence intensified by the inner filter effect (IFE) with AuNPs, allowing for rapid and sensitive CEA detection in human serum, detailed in Fig. 3(III)A and B.

Real-time data processing and sharing capabilities are invaluable for remote healthcare and in areas with limited access to medical infrastructure, positioning this technology as a breakthrough in point-of-care (POCT) diagnostics. Furthermore, the incorporation of such perovskite-based mobile camera technology with cloud computing and AI, as implemented in Li *et al.*'s cloud-fingerprint operation platform (FOP), showcases a transformative approach to data processing and personal identification.[99] The system, which employs high-definition luminescent fingerprint (LFP) imaging, optimizes the synthesis of $CsPbBr_3$ NCs to enhance identity verification processes, significantly boosting the efficiency of forensic case handling, as shown in Fig. 3(IV)A–C. This novel strategy not only elevates the performance of analytical devices but also ensures that complex analyses, once restricted to laboratories, can now be conducted directly at the point of care.

2.3. High electroluminescence quantum efficiency

Perovskite-based nanomaterials are at the forefront of ECL sensor development due to their excellent optoelectronic properties,[111–114] including direct bandgap,[115] robust defect tolerance,[116] and tunable emission. ECL research in perovskite-based nanomaterials is advancing, showcasing diverse applications and efficiencies across various types of perovskites (detailed in Table 3). For instance, $MAPbBr_3$ microcrystals (MCs) sandwiched between ITO-coated glass plates, show potential in LEDs and solar cells, with an external quantum efficiency (EQE) of 45.5% and emission at 525 nm and 560 nm. 2D $CsPbBr_3$ layers, used in blue LEDs, have a lower EQE of 12.2%. ZnO/PEIE/perovskite/TPBi/LiF/Al layered structures, emitting at 799 nm, show promise for near-infrared (NIR) LEDs with an EQE of 21.3%. Yb_{3+}: $CsPb(Cl_{1-x}Br_x)_3$ nanocrystals (NCs) and PEABr:$CsPbBr_3$ films, both used in NIR LED applications, demonstrate EQEs of 7.7% and 16.3%, respectively. The PET-ITO/PEDOT: PSS/PTAA/$CsPbX_3$ QDs/TPBi/LiF/Al architecture, designed for inkjet-printed quantum dot LEDs (QLEDs), achieves an EQE of 23%. In addition, MSPE-$FAPbI_3$ based films, applied in electrically pumped lasers, also reach an

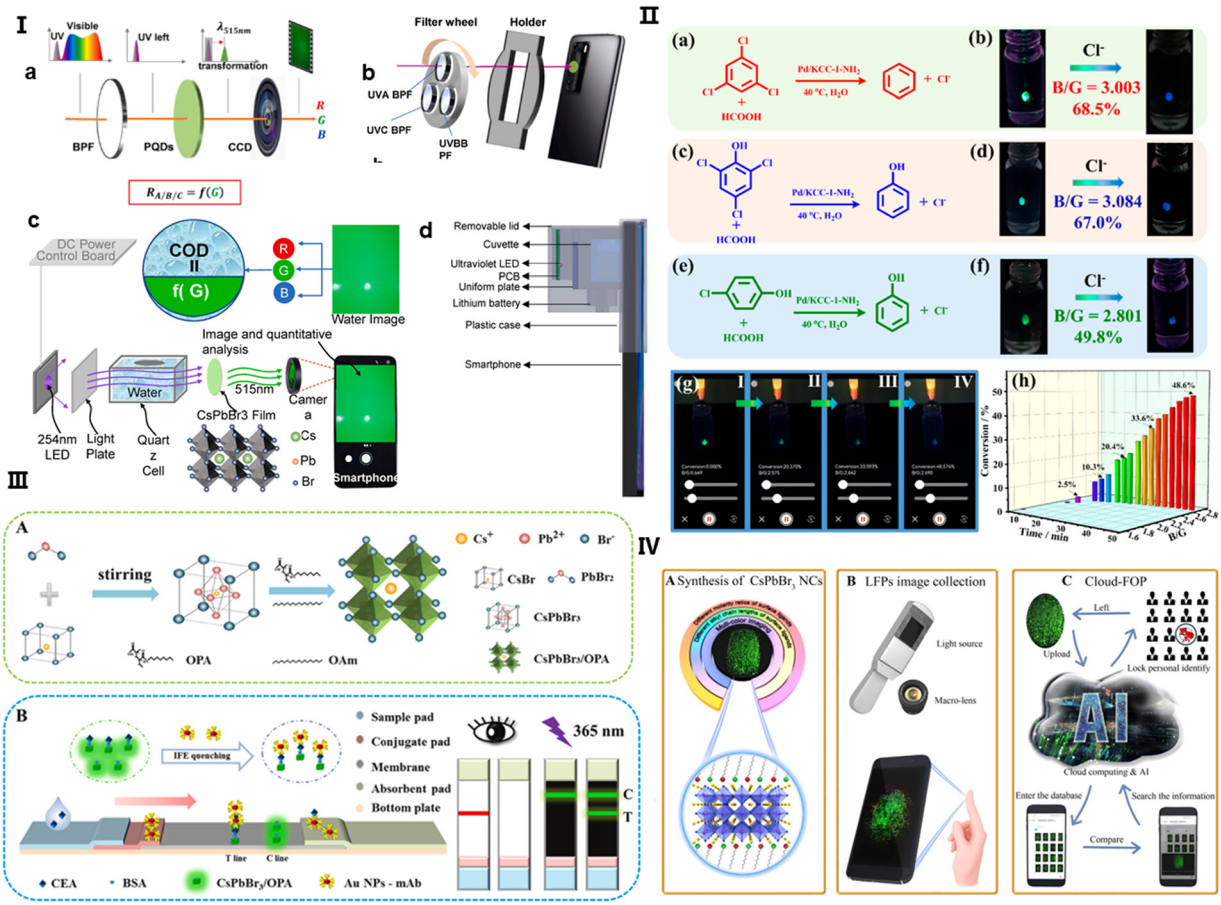

Fig. 3 (I) (a) Diagram illustrating the operation of a UV sensor with a perovskite quantum dot (QD) layer used for color conversion, positioned in front of a smartphone camera. The sequence of light transmission involves a bandpass filter, a perovskite QD liquid layer, and the camera, converting UV wavelengths to visible light for detection by the camera. (b) A representation of the sensor design, featuring a filter wheel with three bandpass filters for UVA, UVB, and UVC selection, a smartphone equipped with perovskite QDs on its camera, and a holder linking the filter wheel to the phone. (c) The sensor's working principle: UV light from a 254-nm LED is absorbed by the water sample, transformed into green light by the perovskite QDs on the camera, with water chemical oxygen demand (COD) assessed through light absorbance. Adapted with permission.[96] Copyright 2023, Elsevier. (II) (a), (c) and (e) Illustrations of the dechlorination processes for different chlorinated compounds. (b), (d) and (f) The corresponding visual detection using $CsPbBr_3$@MOF-5 composites for fluorescence with recorded blue/green (B/G) values. (g) An android app interface showcasing real-time monitoring of dechlorination. (h) A graph tracking the B/G value changes over time, reflecting the dechlorination of 2,4,6-trichlorophenol. Adapted with permission.[97] Copyright 2023, American Chemical Society. (III) (A) A schematic for the synthesis of $CsPbBr_3$/oleylamine (OPA) nanocrystals (NCs). (B) A diagram showing the dual-signal lateral flow immunoassay (LFIA) using $CsPbBr_3$/OPA NCs and AuNPs for concurrent CEA detection. Adapted with permission.[98] Copyright 2024, Elsevier. (IV) The process flow: (A) synthesis of $CsPbBr_3$ NCs with customizable features, (B) acquisition of LFP images using a fluorescence excitation source, a macro lens, and a smartphone, and (C) cloud-based feature extraction for LFP analysis. Adapted with permission.[99] Copyright 2020, American Chemical Society.

EQE of 23%. These advancements reflect the growing versatility and efficiency of perovskite-based materials in ECL research, spanning from optoelectronics to laser applications.

These attributes are critical in the development of highly sensitive and selective sensors for a broad array of analytes.[117] Recent progress in perovskite nano structuring has successfully enhanced charge confinement, which is essential for boosting QY and electroluminescent quantum efficiency (EQE), especially in low-power and sensitive applications.[118–120] Some sizable electrochemical workstations that can be run by smartphones, have undergone significant transformation toward more compact and user-friendly formats.[121,122] An important development in this area is a portable ECL system integrating smartphone imaging and machine learning for the detection of analytes like nitrofurazone (NFZ) (Fig. 4).[123] This system capitalizes on the increased surface area of Ag^+@UiO-66-NH_2 combined with $CsPbBr_3$ nanomaterials, improving both the loading capacity and detection potential. Investigations into the ECL responses of various modified electrodes reveal that the ECL intensity follows the order: bare glassy carbon electrode (GCE) < UiO-66-NH_2 < Ag@UiO-66-NH_2 < $CsPbBr_3$ < UiO-66-NH_2/$CsPbBr_3$ < Ag@UiO-66-NH_2/$CsPbBr_3$, with the presence of $S_2O_8^{2-}$ in PBS solution, and an additional increase with NFZ due to its co-reaction promoting effect. The reduction of NFZ enhances the generation of $SO_4^{\bullet -}$, an oxidizing species, thus amplifying the ECL signal. The Ag^+@UiO-66-NH_2/$CsPbBr_3$/MIP/GCE

Table 3 Overview of ECL properties of Perovskites and their potential applications as described in various references

Perovskite involved	Fabrication	Applied voltage/ Excitation/Emission	Device parameters or efficiency	Application	Ref.
$CsPbBr_3$ film	A single $CsPbBr_3$ MW connects two SWCNT film electrodes	4.5–7 V/490 nm/521 nm	Frequency: 10 Hz; voltage: 6 V; duty cycle: DC 30%; illumination intensity: 6 mW cm^{-2}.	Optoelectronic devices	124
$MAPbBr_3$ MCs	Sandwiching $MAPbBr_3$ MCs in between two ITO-coated glass plates	5–10 V/460 nm/ 525 nm, 560 nm	EQE:45.5%	LEDs and solar cells	125
2 D $CsPbBr_3$ layers	One-step spin coating using precursors: $CsPbBr_3$:MeCl:$EDBr_2$.	2–6 V/405 nm/472–482 nm	EQE:12.2%	Blue LEDs	126
ZnO/PEIE/perovskite/ TPBi/LiF/Al layers	The layers were spin-coated on the ITO substrate	4 V/532 nm/799 nm	EQE:21.3%	NIR LED	127
Yb^{3+}: $CsPb(Cl_{1-x}Br_x)_3$ NCs	The perovskite films were spined coated on ITO glass	3.2 V/400 nm/990 nm	EQE:7.7%	NIR LED	128
PEABr:$CsPbBr_3$ film	The films were spined coated on ITO glass	4–7 V/400 nm/510 nm	EQE:16.3%	LED and laser	129
PET-ITO/PEDOT: PSS/PTAA/$CsPbX_3$ QDs/TPBi/LiF/Al	The multilayer architecture was printed on ITO	4 V/365 nm/515 nm	EQE:23%	Inkjet-printed QLEDs	130
MSPE-$FAPbI_3$ based films	The perovskite layer was spin-coating on modified ITO substrates	4.4 V/405 nm/800 nm	EQE:23%	Electrically pumped lasers	131

MW, microwire; MCs, microcrystals; PEABr, phenethyl ammonium bromide

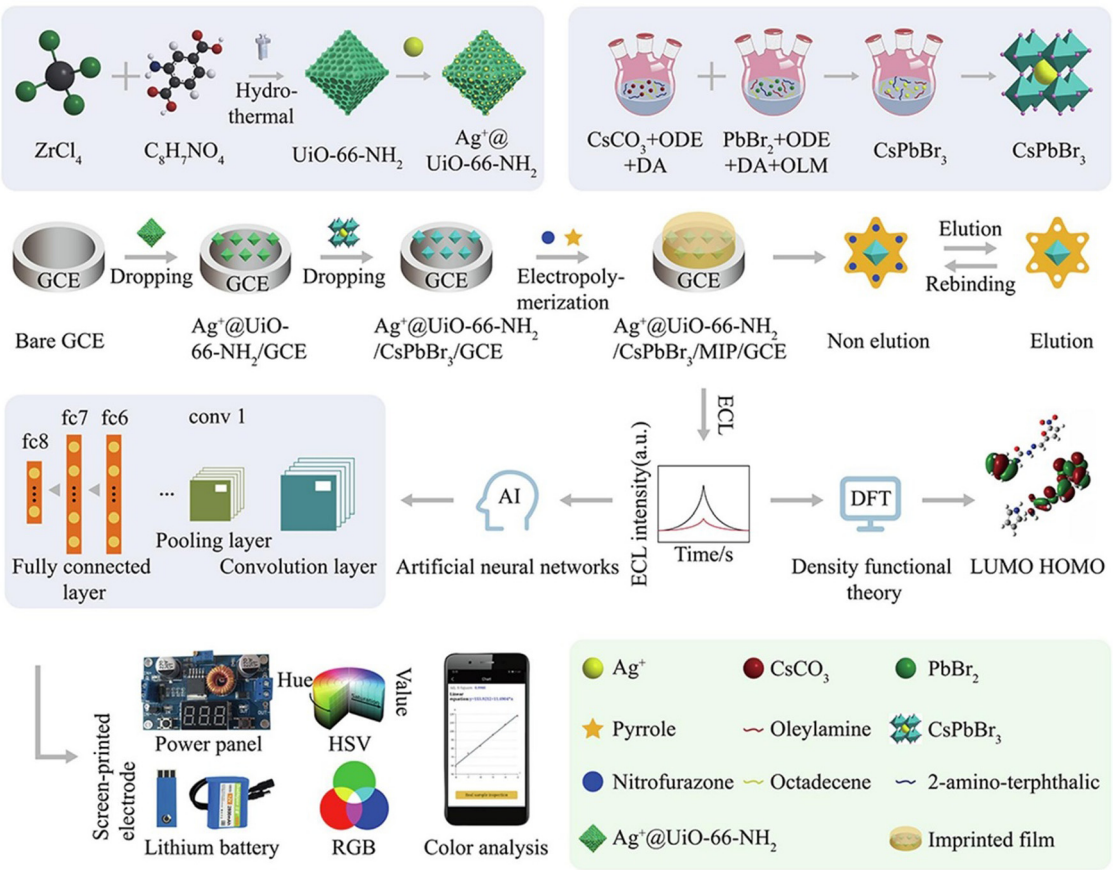

Fig. 4 A comprehensive illustration of the Ag^+@UiO-66-NH_2/$CsPbBr_3$/MIP/GCE assembly for a mobile smartphone-based electrochemiluminescence molecularly imprinted polymer (ECL-MIP) system, depicting the intricate steps of preparation, integration of machine learning techniques, and the sensing mechanism. Adapted with permission.[123] Copyright 2022, Elsevier.

sensor, as a result, shows remarkable anti-interference performance, high sensitivity, and a linear response to NFZ across a broad concentration range with a notably low detection limit. The integration of machine learning optimizes the sensor's accuracy, providing a robust tool for real-time, on-the-spot analytical applications, which could revolutionarily influence environmental and health diagnostics.

As the field of smartphone-based optical sensing with perovskite-based nanomaterials evolves, future research may emphasize enhancing sensor sensitivity and selectivity, crucial for detecting a broader range of analytes with greater precision. This involves refining perovskite structures and compositions to tailor detection capabilities for specific targets, a key step in expanding applications in environmental monitoring and healthcare. Sustainability also plays a critical role, where research must focus on eco-friendly synthesis of perovskites, sustainable manufacturing processes, and the lifecycle impact of these sensing system, including recycling options. Additionally, integrating these sensors with other technologies like wearable devices or IoT systems could offer continuous monitoring capabilities, opening possibilities for comprehensive environmental and health diagnostics.

3. Photothermal-pyroelectric sensors

In the field of smartphone-assisted health diagnostics, some nanomaterials are critical in enhancing photothermal-pyroelectric biosensors (PPBs), which employ both the photothermal effect-converting light to heat-and the pyroelectric effect-producing electric charge in response to temperature changes. The performance of PPBs, notably their sensitivity and specificity, is highly dependent on the choice of nanomaterials for precise biological marker detection. For instance, Au NPs are effective in photothermal conversion but may lack strong pyroelectric properties. Carbon-based nanomaterials excel in electrical conductivity and surface area but may not perform as well in photothermal efficiency. Silicon–water heterojunction photodetectors have the potential for self-powered, broad-spectrum detection but might be surpassed by the stability and response rates of perovskite-based alternatives.[132] Perovskites are distinguished by their significant photothermal responses and excellent pyroelectric characteristics (as detailed in Table 4). For instance, the Au/$BaTiO_3$ hybrid nanostructures demonstrate the potential of enhancing thermal-plasmonic coupling, crucial for accelerated pyro-catalytic hydrogen production. The ITO/$BA_2MA_{n-1}Pb_nBr_{3n+1}$/$PC_{61}BM$/Bi/Ag material showcases an impressive increase in photocurrent, lending itself to applications in wearable devices and wide-range spectral sensing. Similarly, $(IA)_2(EA)_2Pb_3Cl_{10}$ exhibit a broadband photo-pyroelectric effect, promising for high-performance infrared photodetectors. The C-PVDF-BTO combination emphasizes precise heat targeting and eco-friendliness in energy sources. tBT@PDA NPs introduce an integrated approach for photothermal-photodynamic therapy and antibiotic therapies, while PbI_2/$Pb(SCN)_2$-TMIMI highlight advancements in photodetection with improved stability and responsivity. Each of these developments underscores the multi-faceted potential of nanomaterials in enhancing the capabilities and applications of PPBs in various fields, including healthcare, environmental monitoring, and energy efficiency.

They can absorb specific light frequencies to match the narrow spectral output of smartphone light sources, rendering them ideal for biosensing applications, as discussed in conjunction with Fig. 5. A state-of-the-art photothermal-pyroelectric sensing platform has been constructed, featuring a ZnO/$AgBiS_2$-doped heterojunction on a flexible polyimide-paper-based electrode, enhanced by oxygen-deficient $SrTiO_3$ (Fig. 5a(A) and (B)). This setup optimizes charge transfer, boosting photoelectric performance under NIR laser exposure. The interaction with a target molecule activates the Cas12a-crRNA complex, diminishing photocurrent in a way that promotes the biosensor's efficacy in point-of-care diagnostics. The proposed charge transfer mechanism within this heterostructure is detailed in Fig. 5b(A–D). The strategic positioning of energy bands facilitates efficient charge transfer, mitigated by a built-in pyroelectric field, leading to a robust photoelectric response. This field, affected by photothermal influences, prompts the transfer of photoexcited charges within the heterostructure, substantially minimizing charge recombination and enhancing carrier transport rates.

These nanomaterials may be capable of absorbing light and converting it into heat (photothermal effect), subsequently leading to a change in temperature. This temperature change can induce a pyroelectric effect in certain materials, generating an electric current or voltage. By harnessing these properties, perovskite-based nanomaterials could potentially detect and monitor specific biological substances or changes within the body. This process involves the nanomaterials reacting to targeted substances, leading to localized temperature changes which are then translated into measurable electrical signals.

For practical uses like cardiac monitoring, perovskite-based PPBs can be seamlessly integrated into smartphone accessories. This technology translates the thermal response to cardiac biomarkers into an electrical signal processed by a smartphone app, enabling user communication. A device IPPBA for detecting cardiac troponin I (cTnI), leveraging photothermal-pyroelectric transduction and enzymatic amplification for rapid detection (Fig. 5c(A–D)) has been developed. It offers advantages over traditional assays, including ELISA, in terms of speed, cost, and adaptability to various settings. Fig. 5d depicts the variable-temperature pyroelectric effect, demonstrating how dipole alignment and resulting pyroelectric current generation respond to temperature changes. In a pyroelectric material, spontaneous polarization induces two potential surfaces, attracting charge carriers at an electrode interface or in an ionic solution, thereby altering the dipole balance due to temperature variations-a principle utilized in real-time diagnostic tools. Smartphones bolster the function of PPBs through computational power and connectivity, facilitating on-the-spot data analysis and health monitoring, which is critical for real-time healthcare communication and

Table 4 Advantages of utilizing Perovskite materials in photothermal, pyroelectric, and combined application scenarios

Platform	Sample fabrication	Advantages	Potential applications	Effect	Ref.
PE/ZnO/$AgBiS_2$/$SrTiO_3$	*In situ* ZnO/$AgBiS_2$ heterojunction on PE *via* ion-exchange; localized $SrTiO_3$ with oxygen deficiency onto ZnO/$AgBiS_2$/PE.	Addresses the impact of temperature variation on the platform; shows synergy between NIR-induced photothermal and pyroelectric effects	Enables precise target quantification *via* let–7a-regulated CRISPR–Cas12a	Photothermal-pyroelectric	133
IPPBA	Synthesis of $NaNbO_3$ *via* hydrothermal process; spin-coated onto electrode; ultrasonic treatment pre-testing for nanoparticle adherence.	Enhanced detection sensitivity through enzymatic amplification and pyroelectric conversion; integration of capacitor for amplified signal consolidation	Quick detection of cTnI in POC test	Photothermal-Pyroelectric	134
Au/$BaTiO_3$ hybrid nanostructures	Hydrothermal synthesis of coral-like $BaTiO_3$ NPs; *in situ* Au NP coating on $BaTiO_3$	$BaTiO_3$/Au NPs enhance thermal-plasmonic coupling; pulsed laser for rapid localized heating and cooling; synergistic effect boosts catalytic effects.	Accelerated pyro-catalytic hydrogen production	Pyroelectric	135
ITO/$BA_2MA_{n-1}Pb_nBr_{3n+1}$/$PC_{61}BM$/Bi/Ag	ITO prepared; PEIE-treated for surface optimization; spin-coated perovskite; cleaned/healed films; $PC_{61}BM$ layer added; Bi/Ag layers thermally evaporated	67.8x increase in peak-to-peak photocurrent; high reproducibility; stable in 80 ± 5% humidity and 80 °C temperature for 32 days.	Wearable device, wide-range spectral sensing, rapid optoelectronic detection, and imaging.	Pyro-phototronic effect	136
$(IA)_2(EA)_2Pb_3Cl_{10}$	confining EA in cavities as $(IA)_2(EA)_2Pb_3Cl_{10}$ and the crystals were obtained by a temperature cooling method	Broadband photopyroelectric effect covering UV to NIR-II (266–1950 nm)	Promising for high-performance infrared photodetectors	Photopyroelectric	137
C-PVDF-BTO	Spin-coated BTO NPs in PVDF/acetone-DMF on glass; transparent PVDF–BTO membrane after curing; smooth side and rough side with BTO NPs. Sprayed CB powder for solar absorption	Facilitates high-temperature catalytic reactions; maximizes energy efficiency by targeting heat precisely where it's needed in catalysis;	Precise heat targeting; eco-friendly energy source	Photothermal-pyroelectric	138
tBT@PDA NPs	Preparation: Partial PDA coating on tBT nanoparticles; drug loading: ciprofloxacin (CIP) on PDA caps	PTT: boosts thermophoresis, overcomes ROS limitations; pyroelectric field: disrupts membranes, enhances antibiotic uptake	Produced integral PTT/PEDT/antibiotic therapies	Photothermal-pyroelectric	139
PbI_2/$Pb(SCN)_2$-TMIMI	$MAPbI_3$ film creation with hot spin-coating and MAAc solvent; large grain, consistent orientation; PbI_2 partly replaced by $Pb(SCN)_2$; $TMIMPbI_3$ added to $MAPbI_3$ for 1D/3D film	Enhanced photo-sensing with 6.6 mA/W responsivity; reduced carrier recombination; improved pyro-phototronic effect; anti-humidity stability	Wearable or portal optoelectronics	Photothermal-pyroelectric	140

PE, polyimide-paper-based electrode; IPPBA, integrated photothermal-pyroelectric biosensor for AMI; cTnI, cardiac troponin I; 2D RP perovskite films, $(BA)_2(MA)_{n-1}Pb_nBr_{3n+1}$, $\langle n \rangle$ =2–5; PDs, photodetectors; RP, Ruddlesden–Popper; PC61BM, [6,6]-phenyl C61 butyric acid methyl ester; PEIE, polyethylneimine; BTO NPs, $BaTiO_3$ NPs; PVDF, polyvinylidene difluoride; Janus tBT@PDA NPs, capping polydopamine (PDA) on tetragonal $BaTiO_3$ (tBT) NPs, followed by ciprofloxacin (CIP) loading on the PDA caps

record-keeping. Understanding and leveraging perovskite-based nanomaterials for medical diagnostics and monitoring is challenging due to the intricate nature of human biological systems and the complex interactions between these nanomaterials and target substances. Advancement in this field begins with the careful surface modification or functionalization of the nanomaterials, a critical process that enables selective binding to specific biomolecules in the human body. Functionalization is achieved through various chemical methods or by attaching molecules with strong affinity for the targets.

Once bound to these functionalized surfaces, exposure of the perovskites to specific light wavelengths triggers a photothermal effect, causing a localized temperature increase that facilitates the release of the adsorbed substances for detection. This detection leverages the photopyroelectric effect, wherein the perovskite nanomaterials, upon illumination, generate electron–hole pairs due to their optoelectronic properties. The interaction of these pairs with the released substances induces changes in the nanomaterials' electrical properties, enabling precise monitoring of various biomolecules or chemical substances using a smartphone, a significant step forward in medical diagnostics and biosensor applications.

Further development of these perovskite-based hybrid nanostructures for practical sensing applications requires ensuring their stability, high photothermal responses, and effective pyroelectric performance. This entails a comprehensive strategy including the strategic design of nanostructures to enhance light absorption and heat conversion for improved photothermal efficiency. Selecting appropriate constituent materials is essential to augment the perovskite's properties and overall performance. Interface engineering, crucial for charge transfer efficiency, necessitates molecular-level optimization to ensure efficient charge separation and transport. Doping and modulation with specific ions or molecules enhance stability and functional properties, particularly for pyroelectric performance. Optimizing synthesis and fabrication processes is key to

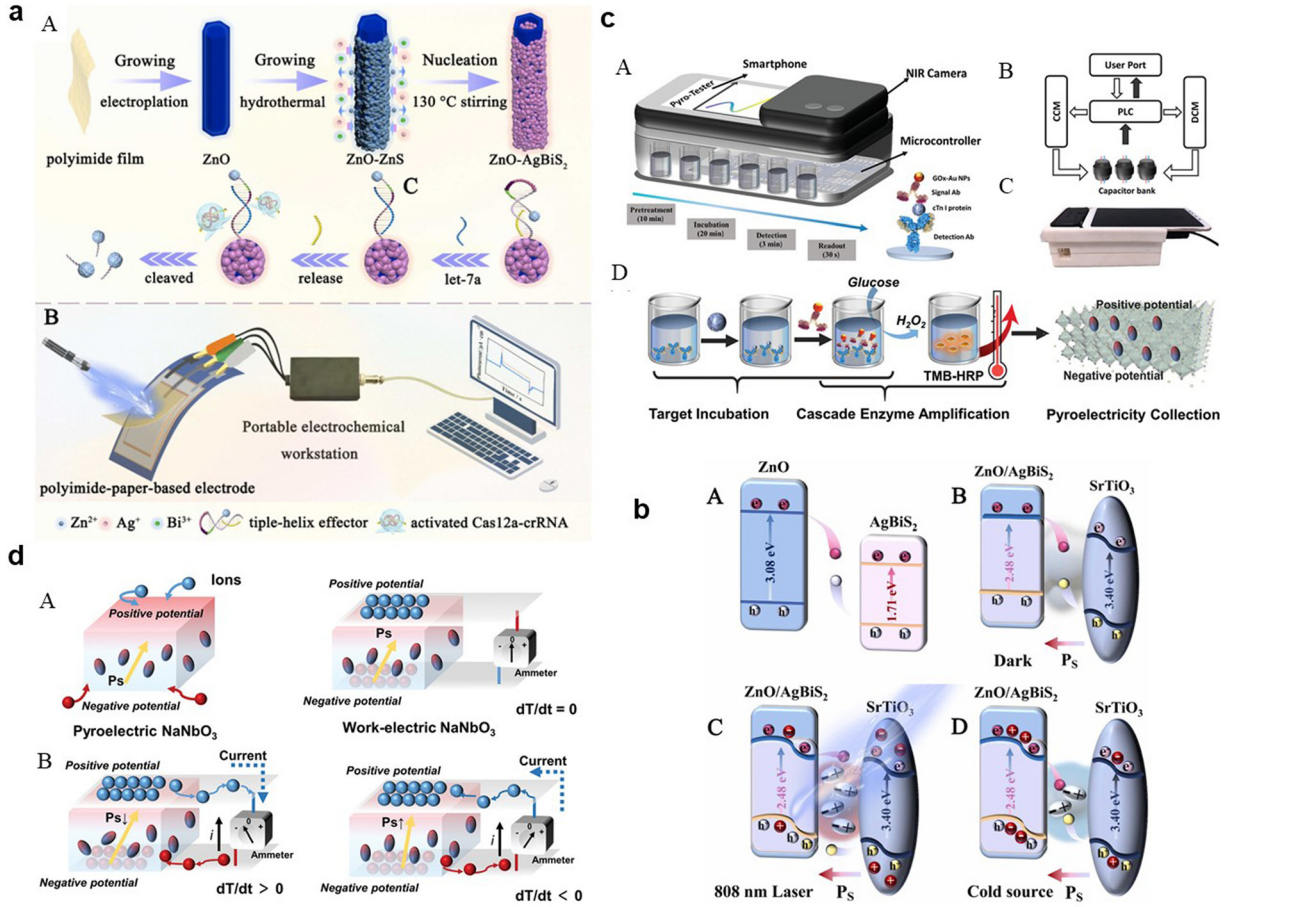

Fig. 5 (a) Illustrative diagram of the photothermal-pyroelectric sensing platform: (A) setup process and (B) operational procedure; (b) depiction of the NIR-responsive enhancement in photoelectrochemical performance due to photo-induced carrier activity: (A) carrier movement in the default state, (B) carrier flow with $SrTiO_3$ present without 808 nm laser activation, (C) intensified oscillation of pyroelectric field dipoles under photothermal influence with 808 nm laser, and (D) reorientation of dipoles when the 808 nm laser is off. Adapted with permission.[133] Copyright 2023, Elsevier. (c) Comprehensive layout of the photothermal-pyroelectric bioassay system: (A) structural diagram, (B) depiction of signal conversion and collection using a commercial capacitor array and microcontroller, (C) actual images of the IPPBA system, (D) Process illustration of target incubation, cascade enzymatic amplification, and photothermal-pyroelectric signal conversion; (d) graphical representation of potential shifts and pyroelectric activity in a thermally stimulated thermoelectric element: (A) polarization process in a pure-phase pyroelectric material and the induced electric field across the phase interface with electrodes, (B) potential electron transfer routes in pyroelectric materials upon thermal excitation. Adapted with permission.[134] Copyright 2022, Wiley-VCH.

achieving desired stability and functionality. Encapsulation techniques protect the nanostructures from environmental factors, maintaining their photothermal and pyroelectric properties. Regular characterization and monitoring are vital to understand behavior under different conditions and to identify any degradation mechanisms. A multifaceted approach, tailored to each application's specific requirements and the materials' inherent characteristics, is fundamental in developing these nanostructures for enhanced stability, efficient photothermal response, and robust pyroelectric performance.

4. Advancements in wearable device

As we delve into the latest advancements in wearable devices, a key focus is on the innovative use of perovskite-based nanomaterials. These materials may be revolutionizing the field due to their unique optoelectronic properties, such as flexibility, stretchability, and lightness.

Perovskite-based nanomaterials are emerging as a transformative element in the realm of wearable devices, primarily due to their remarkable optoelectronic properties, including flexibility, stretchability, and lightweight nature.[141–143] These features make perovskite devices ideally suited for wearable technology, capable of continuous monitoring of vital health metrics such as glucose levels, pH, sodium ion concentrations, sweat rate, and skin temperature, which are crucial for comprehensive health and fitness monitoring.[144–146] The economic viability of perovskite-based technologies is enhanced by their low-cost manufacturing and ease of production. Moreover, the tunable bandgap of these materials facilitates customized applications in diverse devices and is key to adapting to

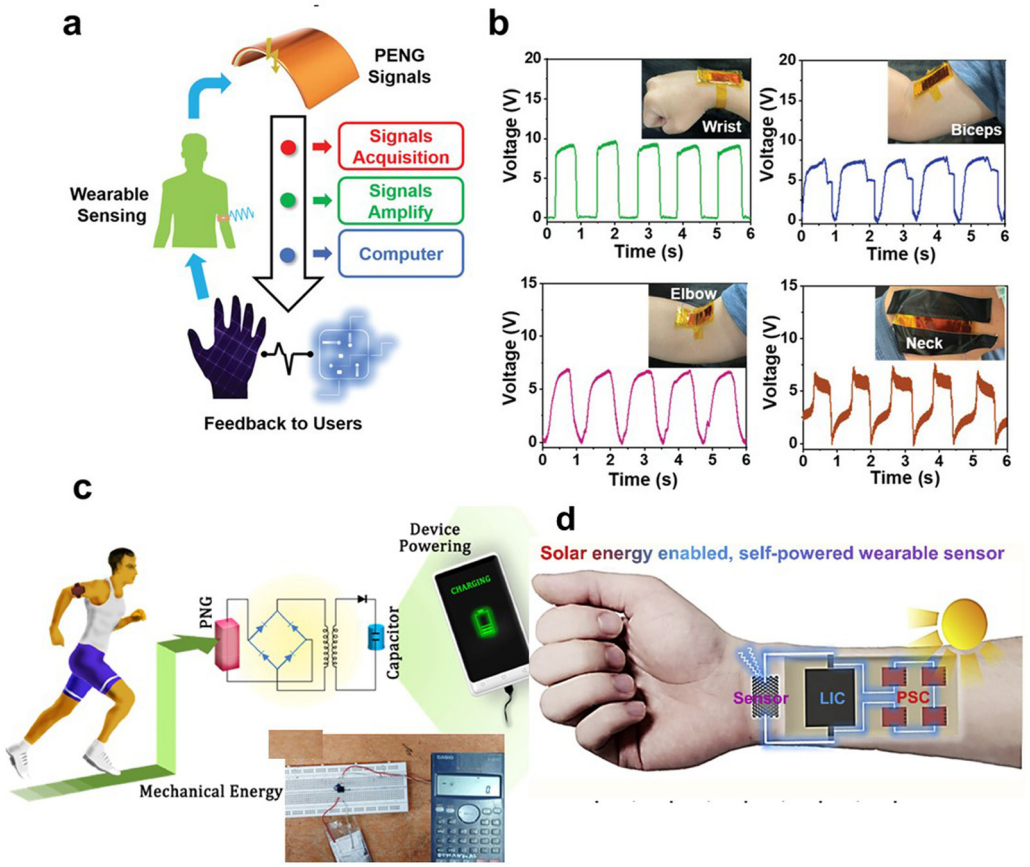

Fig. 6 Exploring the use of piezoelectric stretchable composites (PSC) in wearable Technology: a case study with micro/nano piezoelectric generators (MN-PENGs). (a) Diagrammatic representation of how the human-machine interface functions. (b) Graphs showing voltage outputs generated from movements at the wrist, biceps, elbow, and neck. Adapted with permission.[149] Copyright 2022, Wiley-VCH. (c) Depiction of a biomechanically-powered portable charger: Incorporating a piezoelectric nanogenerator (PNG) within a shoe sole for device charging. Adapted with permission.[150] Copyright 2022, Elsevier. (d) Schematic representation of a self-powered wearable sensor system enabled by Sol Energy (integration of PSC-LIC sensor). Adapted with permission.[152] Copyright 2019, Elsevier.

varying lighting conditions, crucial for wearable sensors.[147,148] For instance, Wu *et al.* showcased a human-machine interface by applying metal-free perovskite (MDABCO-NH_4I_3) films, highlighted in Fig. 6a, which facilitates real-time interaction *via* signal processing.[149] Fig. 6b demonstrates the MDABCO-NH_4I_3-based piezoelectric nanogenerator (MN-PENG)'s ability to generate power from diverse body movements, including wrist and neck. Additionally, a sophisticated gesture recognition system using five MN-PENGs was developed, each representing a different finger on a glove, capable of recognizing five unique gestures (''one'' to ''five''). These gestures are visually displayed on a computer interface, illustrating MN-PENG's utility in self-powered sensors and human–machine interfaces. The MN-PENG, being metal-free, stable, non-toxic, and flexible, holds promise for future wearable and portable therapeutic devices. Mondal *et al.*'s research, which integrates chemically processed $CsPbCl_3$ into a polyvinylidene difluoride (PVDF) matrix, showcases perovskite's utility in energy harvesting, enhancing wearable devices' performance for functions like posture correction and portable charging.[150] Their technology, depicted in Fig. 6c, harnesses biomechanical movements to generate electrical energy, signifying a step forward in powering low-wattage devices and addressing the constraints of conventional batteries. Min *et al.* report on a self-powered wearable biosensor that employs a flexible perovskite solar cell (FPSC) for continuous metabolic monitoring.[151] This device, remarkable for its autonomous operation, extracts and analyzes sweat using an FPSC notable for its high-power conversion efficiency-14.00% in sunlight and 29.64% under indoor lighting. It demonstrates the potential for over 12 hours of uninterrupted function in various lighting conditions without the need for external power or intense activity, thanks to the perovskite material's high absorption coefficient, tunable bandgaps, and long electron and hole diffusion lengths. Li *et al.* have leveraged these properties in a perovskite solar cell driven photo-rechargeable lithium-ion capacitor (PSC-LIC) system-powered sensor that operates independently of external power sources, as shown in Fig. 6d.[152] This sensor, is distinguished by its flexible layered heterostructure, proving effective in monitoring physiological signals such as pulse and movement. Such developments enable long-term, autonomous health tracking.

Table 5 Utilization of Perovskite-Based nanomaterials in the development of wearable devices

Device based	Perovskite or the composite involved	Role of perovskite	Application realized	Ref.
Shadow recognition sensor	LC-PVK; $MAPbI_3$	Absorbs sunlight fully, converting it into electron–hole pairs for enhanced photoelectric efficiency	The perovskite photovoltaic sensor first captures and digitizes tag brightness, then a Python program analyzes the data in real-time for gesture segmentation.	153
Biomechanical monitoring sensor	CPB-K/PDMS TENG; $CsPbBr_3$-KBr	Enhancing triboelectric nanogenerators	Physiological signals vary across different body parts and under various stimuli; collecting these signals by the sensor enables the detection of human motion.	154
Cholesterol PEC sensor	TiO_2 IOPCs/$MAPbBr_3$; $CH_3NH_3PbBr_3$	Photogenerated electrons were more easily transmitted from the conduction band of $CH_3NH_3PbBr_3$ QDs to the ITO surface through the TiO_2 layer	The sensor detects cholesterol by capturing it in MIPs, which reduces photocurrent due to hindered electron transfer.	155
Breath monitoring mask	$Cs_3Cu_2I_5$	Humidity-sensitive	The mask's sensor adjusts its resistance to reflect breathing patterns upon use, and humidity inside the mask drops to over 90% RH within 3 seconds of wearing.	156
Gesture recognition sensor	$CsPbBr_3$	Shortening conduction distance and boosting photoelectric conversion efficiency	The sensor detects photocurrent changes due to finger movement on a flexible, transparent PET substrate with perovskite film, facilitating gesture-based input for devices like smartwatches.	157
TC fluorescence sensor	$CsPbBr_3$@Cs_4PbBr_6@NH_2@Eu	A core component in a multicolor fluorescent nano sensor	The sensor works by using an agarose gel with a fluorescent biosensor on gloves, which changes color from green to red under UV light to detect TC	158
Blood oxygen sensor	$Cs_{0.05}MA_{0.45}FA_{0.5}Pb_{0.5}Sn_{0.5}I_3$	Create a photoactive layer within Sn–Pb photodetectors, crucial for efficient photocarrier separation and collection	The sensor works by using Sn–Pb perovskite photodetectors to non-invasively monitor heart rate and blood oxygen saturation through photoplethysmography	159

LC, liquid crystal; LC-PVK, LC-doped $MAPbI_3$ film; CPB-K, $CsPbBr_3$-KBr microcrystals; PDMS, polydimethylsiloxane; TENG, triboelectric nanogenerator; PEC, photoelectrochemical; TiO_2 IOPCs, titanium dioxide inverse opal; TC, tetracycline

The profound implications of PSCs in the realm of wearable technology extend considerably beyond their current applications (detailed in Table 5). Characterized by a high absorption coefficient, tunable bandgaps, and prolonged electron and hole diffusion lengths, these perovskites exhibit a remarkable degree of versatility and adaptability to diverse lighting environments. This adaptability harbors the potential to revolutionize the interaction paradigm with personal electronic devices, emancipating them from the constraints of perpetual charging and limited battery lifespan. Nonetheless, the path to the widespread integration of perovskite in wearable technology is fraught with significant environmental and health challenges, particularly concerning the lead content inherent in these cells. These challenges transcend mere technical obstacles, posing profound ethical quandaries. They necessitate a rigorous scrutiny of the materials employed in the technological vanguard, compelling a reassessment of the balance between innovation and sustainability. The resolution of these issues is critical not only to the technical viability of perovskite-based wearables but also emblematic of a broader commitment to harmonizing technological advancement with ecological prudence and health conscientiousness. These advancements not only signify progress in wearable device technology but also highlight the need to address environmental and health challenges, especially concerning the lead content in these materials. The path ahead for perovskite-based wearables involves navigating the balance between innovation, environmental responsibility, and ethical considerations.

5. Prospect and conclusions

In summary, we've detailed the transformative impact of perovskite-based nanomaterials evolving smartphone-based sensors. These materials, having exceptional optical properties, photothermal-pyroelectric effects, and flexible structure, substantially enhance sensor functionalities. This advancement allows for the accurate conversion of complex biological activities into quantifiable electrical and optical signals, vital for real-time health diagnostics. Integrating perovskite-based nanomaterials into smartphone technology may mark a significant shift, combining laboratory-level precision with the accessibility and convenience of smartphones. We've examined a range of applications, from optical and photothermal-pyroelectric sensing to their potential integration into wearable health monitoring devices.

In the realm of perovskite-based materials, significant advancements have been achieved, yet the field grapples with numerous challenges and untapped potentials. Paramount among these challenges is the question of long-term stability and dependability under variable environmental conditions, such as temperature fluctuations, humidity, and light exposure. The investigation into specific compositions, the application of

protective coatings, development of encapsulation techniques, and exploration of chemical modifications is imperative for augmenting the durability and reliability of these materials, particularly in sensor applications. A further intricate challenge presents itself in the stabilization and prolongation of the lifespan of perovskite-based nanostructures within pliable structures, especially during the processes of folding. This necessitates a multifaceted strategy encompassing structural optimization, for instance, the design of nanostructures capable of enduring mechanical stress through core–shell configurations or integration within flexible matrices. The synthesis and selection of composite materials that harmonize perovskites with pliable substrates are pivotal in enhancing system ductility and durability. Morphological engineering, concentrating on the shape, size, and distribution of nanostructures, is instrumental in mitigating the impacts of mechanical stress. The implementation of protective encapsulation technologies is crucial in safeguarding these nanostructures from environmental and mechanical stressors, thus preserving their flexibility and functionality. Furthermore, exhaustive stress testing and failure analysis, alongside consideration of the variability in perovskite stability, are indispensable for fortifying resilience under real-world conditions. Continuous exploration in novel nanostructures, encapsulation methods, and material amalgamations remains vital for the advancement of perovskite-based nanostructures in the domain of flexible electronics.

Addressing the environmental and health repercussions associated with perovskites, particularly concerning their lead content, is also of paramount importance. Current research is dedicated to probing non-toxic alternatives, diminishing lead content, and devising advanced encapsulation technologies to reduce environmental exposure while retaining perovskite functionality. The establishment of efficacious recycling and reuse protocols, alongside the development of regulatory frameworks and safety guidelines, is essential to manage the utilization and disposal of lead-containing perovskites in a sustainable manner.

Lastly, the integration and upscaling of perovskite-based materials for applications in the smartphone industry pose significant challenges. These encompass emergent manufacturing processes, limited stability, insufficient longevity, and unresolved concerns regarding lead toxicity. To scale up production effectively, it is necessary to optimize production methodologies, develop cost-efficient synthesis techniques, and establish large-scale manufacturing facilities to ensure a high-quality material supply for extensive industrial deployment.

To propel the advancement of sensors in smartphones, the focus should be directed towards technological enhancement through miniaturization and augmented precision, in conjunction with the integration of novel sensor types for health and environmental monitoring. Additional emphasis should be placed on refining AI and data processing capabilities to foster more intelligent application functionalities, as well as on the development of more dynamic user interfaces, such as gesture and voice controls. Further, the expansion of connectivity with other devices and Internet of Things (IoT) systems, coupled with the assurance of robust security and privacy protocols for the data garnered by these sensors, is imperative. The encouragement of application development that ingeniously exploits these advanced sensors is anticipated to broaden the spectrum of applications and ameliorate user experiences.

The journey forward is filled with obstacles, but overcoming them may usher in a new era of accessible, effective, and all-encompassing digital health surveillance, transforming how we approach health monitoring and diagnostics.

Data availability statement

No data was used in the research described in the article.

Author contributions

D. Li contributed to writing the original article, and revision. P. Zhuang contributed to the editing. C. Sun contributed to the supervising of the final manuscript.

Conflicts of interest

There are no conflicts to declare.

Acknowledgements

We acknowledge the financial support from General Project of Natural Science Foundation of Liaoning Province (No. 202304008).

References

1 S. Li, J. Liu, Z. Chen, Y. Lu, S. S. Low, L. Zhu, C. Cheng, Y. He, Q. Chen and B. Su, *Sens. Actuators, B*, 2019, **297**, 126811.
2 F. Li, L. Guo, Z. Li, J. He and H. Cui, *Anal. Chem.*, 2020, **92**, 6827–6831.
3 L. Huang, W. Xiao, T. Xu, H. Chen, Z. Jin, Z. Zhang, Q. Song and Y. Tang, *Sens. Actuators, B*, 2021, **327**, 128893.
4 O. Adeniyi and P. Mashazi, *Microchem. J.*, 2022, **178**, 107427.
5 M. Cui, W. Ling, L. Zhang, Y. Li, J. Liu, T. Sun, B. Ma, S. Lu, H. Pan, G. Pang, Y. Zhang, S. Zhang, X. Huang, P. Zhao, D. Liu and H. Wang, *Chem. Eng. J.*, 2023, **451**, 138812.
6 Y. Xia, J. Hu, S. Zhao, L. Tao, Z. Li, T. Yue and J. Kong, *Biosens. Bioelectron.: X*, 2022, **11**, 100195.
7 Y. Joo, J. Yoon, J. Ha, T. Kim, S. Lee, B. Lee, C. Pang and Y. Hong, *Adv. Electron. Mater.*, 2017, 3.
8 M. Straczkiewicz, P. James and J. P. Onnela, *NPJ Digit Med.*, 2021, **4**, 148.
9 H. Sarmadi, A. Entezami, K.-V. Yuen and B. Behkamal, *Measurement*, 2023, **223**, 113716.
10 A. Roda, E. Michelini, M. Zangheri, M. Di Fusco, D. Calabria and P. Simoni, *TrAC, Trends Anal. Chem.*, 2016, **79**, 317–325.

11 H. Chen, Y. Feng, F. Liu, C. Tan, N. Xu, Y. Jiang and Y. Tan, *Biosens. Bioelectron.*, 2024, **247**, 115929.
12 Q. Gao and S. Li, *IMed*, 2024, e20230031.
13 K. Kim and W. G. Lee, *Small Methods*, 2023, **7**, 2200979.
14 B. Wang, Y. Li, M. Zhou, Y. Han, M. Zhang, Z. Gao, Z. Liu, P. Chen, W. Du, X. Zhang, X. Feng and B. F. Liu, *Nat. Commun.*, 2023, **14**, 1341.
15 S. Qian, Y. Cui, Z. Cai and L. Li, *Biosens. Bioelectron.: X*, 2022, **11**, 100173.
16 H. Zong, Y. Zhang, X. Liu, Z. Xu, J. Ye, S. Lu, X. Guo, Z. Yang, X. Zhang, M. Chai, M. Fan, Y. Liao, W. Yang, Y. Wu and D. Zhang, *View*, 2023, 4.
17 Q. Guo, J. Zhou, K. Hu, Y. He, K. Huang and P. Chen, *Sens. Actuators, B*, 2023, **374**, 132841.
18 Y. Huang, Y. Zhang, W. Hao, H. Lu, H. Dong and X. Zhang, *Sens. Actuators, B*, 2023, **375**, 132945.
19 Q. Lin, Z. Yu, L. Lu, X. Huang, Q. Wei and D. Tang, *Biosens. Bioelectron.*, 2023, **230**, 115260.
20 C. Wang, F. Qin, S. Tang, X. Li, T. Li, G. Guo, C. Gu, X. Wang and D. Chen, *Food Chem.*, 2023, **411**, 135514.
21 Y. Luo, S. Wu, X. Xiang, J. Shu and J. Fei, *Biosens. Bioelectron.*, 2023, **237**, 115525.
22 L. P. Lin and M. T. T. Tan, *Biosens. Bioelectron.*, 2023, **237**, 115492.
23 V. S. K. Cheerala, K. M. Ganesh, S. Bhaskar, S. S. Ramamurthy and S. C. Neelakantan, *Langmuir*, 2023, **39**, 7939–7957.
24 K. Promsuwan, A. Soleh, K. Samoson, K. Saisahas, S. Wangchuk, J. Saichanapan, P. Kanatharana, P. Thavarungkul and W. Limbut, *Talanta*, 2023, **256**, 124266.
25 L. Lu, R. Yu and L. Zhang, *Food Chem.*, 2023, **421**, 136205.
26 Y. Huang, Y. Han, J. Sun, Y. Zhang and L. Han, *Mater. Today Chem.*, 2022, **24**, 100895.
27 R. Gupta, W. J. Peveler, K. Lix and W. R. Algar, *Anal. Chem.*, 2019, **91**, 10955–10960.
28 H. Chen, X. Zhang, Z. Jin, L. Huang, H. Dan, W. Xiao, J. Liang, S. Zou and Y. Tang, *Biosens. Bioelectron.*, 2020, **155**, 112101.
29 J. Zhang and G. Shi, *Anal. Chim. Acta*, 2022, **1198**, 339572.
30 G. H. Darwish, J. Asselin, M. V. Tran, R. Gupta, H. Kim, D. Boudreau and W. R. Algar, *ACS Appl. Mater. Interfaces*, 2020, **12**, 33530–33540.
31 R. Taheri-Ledari, F. Ganjali, S. Zarei-Shokat, M. Saeidirad, F. Ansari, M. Forouzandeh-Malati, F. Hassanzadeh-Afruzi, S. M. Hashemi and A. Maleki, *Energy Fuel*, 2022, **36**, 10702–10720.
32 X. Fang, Z. Chen, Q. Ma, J. Wu, J. Lin, J. Li, W. Li, C. Liu, H. Shen and L. You, *Sol. Energy*, 2023, **262**, 111795.
33 Y. Dong, X. Dong, D. Lu, M. Chen, N. Zheng, R. Wang, Q. Li, Z. Xie and Y. Liu, *Adv. Mater.*, 2023, **35**, 2205258.
34 X. Qiu, J. Xia, Y. Liu, P. A. Chen, L. Huang, H. Wei, J. Ding, Z. Gong, X. Zeng, C. Peng, C. Chen, X. Wang, L. Jiang, L. Liao and Y. Hu, *Adv. Mater.*, 2023, **35**, 2305648.
35 J. G. Cherian, T. Birol, N. C. Harms, B. Gao, S.-W. Cheong, D. Vanderbilt and J. L. Musfeldt, *Appl. Phys. Lett.*, 2016, **108**, 262901.
36 C. H. A. Li, P. K. Ko, C. C. S. Chan, A. Sergeev, D. Chen, N. Tewari, K. S. Wong and J. E. Halpert, *Adv. Funct. Mater.*, 2023, **33**, 2303301.
37 Z. B. Hu, L. H. Li, Y. Han, J. Zhang, J. Li, Z. Chen, S. Wu, Y. Zhang, H. Y. Ye and Y. Song, *Aggregate*, 2022, 4, DOI: **10.1002/agt1002.1294**.
38 T. Kodalle, R. F. Moral, L. Scalon, R. Szostak, M. Abdelsamie, P. E. Marchezi, A. F. Nogueira and C. M. Sutter-Fella, *Adv. Energy Mater.*, 2022, **13**, 2201490.
39 H. Xu, F. Sun, W. Guo, S. Han, Y. Liu, Q. Fan, L. Tang, W. Liu, J. Luo and Z. Sun, *Angew. Chem., Int. Ed.*, 2023, **62**, 202309416.
40 L. Ye, P. Guo, J. Su, K. Zhang, C. Liu, P. Yang, W. Zhao, P. Zhao, Z. Liu, J. Chang, Q. Ye and H. Wang, *Angew. Chem., Int. Ed.*, 2023, **62**, 202300678.
41 D. Moia and J. Maier, *Mater. Horiz.*, 2023, **10**, 1641–1650.
42 Y. Yin, Y. Zhou, S. Fu, X. Zuo, Y. C. Lin, L. Wang, Y. Xue, Y. Zhang, E. H. R. Tsai, S. Hwang, K. Kissenger, M. Li, M. Cotlet, T. D. Li, K. G. Yager, C. Y. Nam and M. H. Rafailovich, *Small*, 2023, **19**, 2207092.
43 I. Ahmad, M. Abohashrh, A. Aftab, H. Aziz, I. Fatima, N. Shahzadi, S. Ahmad and T. Muhmood, *Appl. Mater. Today*, 2023, **32**, 101827.
44 C. Wang, Y. Li, Q. Lv, H. Zheng, G. Zhu, X. Xu and Y. Wang, *Chem. Eng. J.*, 2022, **431**, 134135.
45 S. M. Bukhari and J. B. Giorgi, *Sens. Actuators, B*, 2013, **181**, 153–158.
46 W. Qin, Z. Yuan, Y. Shen, R. Zhang and F. Meng, *Chem. Eng. J.*, 2022, 431.
47 H. Bu, C. He, Y. Xu, L. Xing, X. Liu, S. Ren, S. Yi, L. Chen, H. Wu, G. Zhang, J. Zhao and J. Shi, *Adv. Electron. Mater.*, 2022, **8**, 2101204.
48 J. Casanova-Chafer, R. Garcia-Aboal, P. Atienzar and E. Llobet, *ACS Sens.*, 2022, **7**, 3753–3763.
49 R. Tan, B. Dryzhakov, K. Higgins, J. Charest, Z. Dancoes, P. Kandlakunta, L. R. Cao, M. Ahmadi, B. Hu and E. Lukosi, *ACS Appl. Mater. Interfaces*, 2022, **14**, 34571–34582.
50 M. Guan, Y. Xie, Y. Zhang, Z. Gu, L. Qiu, Z. He, B. Ye, A. Suwardi, Z. Dai, G. Li and G. Hu, *Adv. Mater.*, 2023, **35**, 2210611.
51 D. Spirito, M. Barra-Burillo, F. Calavalle, C. L. Manganelli, M. Gobbi, R. Hillenbrand, F. Casanova, L. E. Hueso and B. Martin-Garcia, *Nano Lett.*, 2022, **22**, 4153–4160.
52 Z. Hu, Y. Jiang, F. Zhou, C. Chen, J. He, Z. Zhan, Z. Liu, J. Du, L. Zhang and Y. Leng, *Adv. Opt. Mater.*, 2022, **11**, 2202131.
53 W. Wu, H. Lu, X. Han, C. Wang, Z. Xu, S. T. Han and C. Pan, *Small Methods*, 2023, **7**, 2201499.
54 L. N. Passini, F. E. Maturi, R. S. Pugina, E. G. Hilário, M. Fontes, H. S. Barud, L. D. Carlos, J. M. A. Caiut and D. Manzani, *J. Mater. Chem. C*, 2023, **11**, 7672–7681.
55 X. Liu, H. Li, Q. Cui, S. Wang, C. Ma, N. Li, N. Bu, T. Yang, X. Song, Y. Liu, Z. Yang, K. Zhao and S. F. Liu, *Angew. Chem., Int. Ed.*, 2022, **61**, 202209320.
56 L. Gurusamy, L. Karuppasamy, S. Anandan, C. H. Liu and J. J. Wu, *Mater. Today Chem.*, 2022, **25**, 100965.

57 T. S. Priya, T. W. Chen, S. M. Chen, T. Kokulnathan, B. S. Lou, W. A. Al-Onazi, A. M. Al-Mohaimeed, M. S. Elshikh and J. Yu, *Chemosphere*, 2023, **318**, 137948.
58 N. Zhou and H. Zhou, *Small Struct.*, 2022, **3**, 2100232.
59 M. J. Seol, S. H. Hwang, J. W. Han, H. W. Jang and S. Y. Kim, *ACS Appl. Electron. Mater.*, 2023, **5**, 5261–5277.
60 J. Wen, Y. Zhao, Z. Liu, H. Gao, R. Lin, S. Wan, C. Ji, K. Xiao, Y. Gao, Y. Tian, J. Xie, C. J. Brabec and H. Tan, *Adv. Mater.*, 2022, **34**, 2110356.
61 J. Ding, L. Gao, L. Cao, Y. Zhou, H. Wang, J. Duan, H. Yin, J. Sun and S. Ai, *Sens. Actuators, B*, 2022, **355**, 131290.
62 S. Huang, L. Tan, L. Zhang, J. Wu, L. Zhang, Y. Tang, H. Wang and Y. Liang, *Sens. Actuators, B*, 2020, **325**, 128751.
63 Q. Wang, C. Xiong, J. Li, Q. Deng, X. Zhang, S. Wang and M. M. Chen, *Food Chem.*, 2023, **410**, 135325.
64 Q. F. Pan, H. F. Jiao, H. Liu, J. J. You, A. L. Sun, Z. M. Zhang and X. Z. Shi, *Sci. Total Environ*, 2022, **843**, 156925.
65 T. Shi, X. Chen, Y. Deng, H. Huang, J. Wang, R. He, Y. Liu, X. He, J. Li, P. K. Chu and X.-F. Yu, *NPG Asia Mater.*, 2022, **14**, 87.
66 Y. Yao, C. Cheng, C. Zhang, H. Hu, K. Wang and S. De Wolf, *Adv. Mater.*, 2022, **34**, 2203794.
67 H. Wu, X. Chen, Z. Song, A. Zhang, X. Du, X. He, H. Wang, L. Xu, Z. Zheng, G. Niu and J. Tang, *Adv. Mater.*, 2023, **35**, 230146.
68 S.-D. Baek, C. Wang, D.-Y. Khang and J.-M. Myoung, *Chem. Eng. J.*, 2023, **455**, 140594.
69 G. Du, L. Yang, C. Zhang, X. Zhang, N. Rolston, Z. Luo and J. Zhang, *Adv. Energy Mater.*, 2022, **12**, 2103966.
70 A. Žužić, A. Ressler and J. Macan, *Ceram. Int.*, 2022, **48**, 27240–27261.
71 H. Zhang, L. Pfeifer, S. M. Zakeeruddin, J. Chu and M. Gratzel, *Nat. Rev. Chem.*, 2023, **7**, 632–652.
72 D. Meng, J. Xue, Y. Zhao, E. Zhang, R. Zheng and Y. Yang, *Chem. Rev.*, 2022, **122**, 14954–14986.
73 Y. Li, H. Xie, E. L. Lim, A. Hagfeldt and D. Bi, *Adv. Energy Mater.*, 2021, **12**, 2102730.
74 Y. Zhan, Q. Cheng, Y. Song and M. Li, *Adv. Funct. Mater.*, 2022, 32.
75 Y. Zhou, L. M. Herz, A. K. Y. Jen and M. Saliba, *Nat. Energy*, 2022, **7**, 794–807.
76 J. He, X. Xu, M. Li, S. Zhou and W. Zhou, *Anal. Chim. Acta*, 2023, **1251**, 341007.
77 L. Kong, X. Zhang, C. Zhang, L. Wang, S. Wang, F. Cao, D. Zhao, A. L. Rogach and X. Yang, *Adv. Mater.*, 2022, **34**, e2205217.
78 D. Liang, Y. Wang and K. Qian, *IMed*, 2023, **1**, e20230020.
79 M. Li, Y. Zeng, X. Qu, M. Jalalah, S. A. Alsareii, C. Li, F. A. Harraz and G. Li, *Small*, 2021, **17**, 2103255.
80 M. Li, Y. Wang, H. Hu, Y. Feng, S. Zhu, C. Li and N. Feng, *Biosens. Bioelectron.*, 2022, **203**, 113979.
81 L. Chen, J. Yang, W. Chen, S. Sun, H. Tang and Y. Li, *Sens. Actuators, B*, 2020, **321**, 128642.
82 X. Wang, W. Cao, L. Qin, T. Lin, W. Chen, S. Lin, J. Yao, X. Zhao, M. Zhou, C. Hang and H. Wei, *Theranostics*, 2017, **7**, 2277–2286.
83 D. Duan, X. Fang and K. Li, *Talanta*, 2022, **240**, 123112.
84 Y. Feng, X. Qu, Y. Peng, X. Xu, J. Zhang, Y. Wang, S. Zhu, M. Li, C. Li and N. Feng, *ACS Appl. Mater. Interfaces*, 2023, **15**, 27742–27749.
85 X. Jiang, X. Wang, A. Lin and H. Wei, *Anal. Chem.*, 2021, **93**, 5954–5962.
86 Q. Ye, E. Yuan, J. Shen, M. Ye, Q. Xu, X. Hu, Y. Shu and H. Pang, *Adv. Sci.*, 2023, **10**, 2304149.
87 X. Wang, X. J. Gao, L. Qin, C. Wang, L. Song, Y. N. Zhou, G. Zhu, W. Cao, S. Lin, L. Zhou, K. Wang, H. Zhang, Z. Jin, P. Wang, X. Gao and H. Wei, *Nat. Commun.*, 2019, **10**, 704.
88 L. Song, Y. Zhu, Z. Yang, C. Wang and X. Lu, *J. Mater. Chem. B*, 2018, **6**, 5931–5939.
89 Y. Chen, W. Nie, Z. Peng, F. Yu, J. Yang and Y. Li, *Sens. Actuators, B*, 2022, **364**, 131869.
90 Q. Zhao, H. Wang, W. Jiang, H. Gao, S. Wen, X. Feng, Q. Wu, C. He, Y. Zhu, L. Hu, B. Zhao and W. Song, *Anal. Chem.*, 2022, **94**, 17930–17938.
91 O. Stroyuk, O. Raievska, J. Hauch and C. J. Brabec, *Angew. Chem., Int. Ed.*, 2023, **62**, 202212668.
92 A. F. Gualdrón-Reyes, S. Masi and I. Mora-Seró, *Trend Chem.*, 2021, **3**, 499–511.
93 M. D. Smith, B. A. Connor and H. I. Karunadasa, *Chem. Rev.*, 2019, **119**, 3104–3139.
94 L. N. Quan, F. P. Garcia de Arquer, R. P. Sabatini and E. H. Sargent, *Adv. Mater.*, 2018, **30**, 1801996.
95 F. F. Gao, H. Song, Z. G. Li, Y. Qin, X. Li, Z. Q. Yao, J. H. Fan, X. Wu, W. Li and X. H. Bu, *Angew. Chem., Int. Ed.*, 2023, **62**, 202218675.
96 H. Tian, L. Jiao, K. Wang, X. Zhao, F. Cao and D. Dong, *Chem. Eng. J.*, 2022, **448**, 137583.
97 Y. Shang, H. Sun, R. Yu, F. Zhang, X. Liang, H. Li, J. Li, Z. Yan, T. Zeng, X. Chen and J. Zeng, *Environ. Sci. Technol.*, 2023, **57**, 11231–11240.
98 Y. Wang, J. Shen, R. Song, Q. Xu, X. Hu and Y. Shu, *Talanta*, 2024, **266**, 125017.
99 M. Li, T. Tian, Y. Zeng, S. Zhu, J. Lu, J. Yang, C. Li, Y. Yin and G. Li, *ACS Appl. Mater. Interfaces*, 2020, **12**, 13494–13502.
100 I. L. Braly, D. W. deQuilettes, L. M. Pazos-Outón, S. Burke, M. E. Ziffer, D. S. Ginger and H. W. Hillhouse, *Nat. Photonics*, 2018, **12**, 355–361.
101 C. Luo, W. Li, D. Xiong, J. Fu and W. Yang, *Nanoscale*, 2019, **11**, 15206–15215.
102 G. Li, H. Wang, T. Zhang, L. Mi, Y. Zhang, Z. Zhang, W. Zhang and Y. Jiang, *Adv. Funct. Mater.*, 2016, **26**, 8478–8486.
103 F. Liu, Y. Zhang, C. Ding, S. Kobayashi, T. Izuishi, N. Nakazawa, T. Toyoda, T. Ohta, S. Hayase, T. Minemoto, K. Yoshino, S. Dai and Q. Shen, *ACS Nano*, 2017, **11**, 10373–10383.
104 X. Li, Y. Wu, S. Zhang, B. Cai, Y. Gu, J. Song and H. Zeng, *Adv. Funct. Mater.*, 2016, **26**, 2435–2445.
105 S. Feng, Y. Ma, S. Wang, S. Gao, Q. Huang, H. Zhen, D. Yan, Q. Ling and Z. Lin, *Angew. Chem., Int. Ed.*, 2022, **61**, 202116511.

106 Y. Tong, E. Bladt, M. F. Ayguler, A. Manzi, K. Z. Milowska, V. A. Hintermayr, P. Docampo, S. Bals, A. S. Urban, L. Polavarapu and J. Feldmann, *Angew. Chem., Int. Ed.*, 2016, **55**, 13887–13892.
107 X. Yang, C. Valenzuela, X. Zhang, Y. Chen, Y. Yang, L. Wang and W. Feng, *Matter*, 2023, **6**, 1278–1294.
108 S. He, Q. Qiang, T. Lang, M. Cai, T. Han, H. You, L. Peng, S. Cao, B. Liu, X. Jing and B. Jia, *Angew. Chem., Int. Ed.*, 2022, **61**, 202208937.
109 X. Ren, H.-L. Hu, Z.-Y. Chen, L.-X. Gao, H. Hao, Y. Liu and F.-L. Jiang, *ACS Appl. Nano Mater.*, 2023, **6**, 6092–6102.
110 X. Hu, Y. Xu, J. Wang, J. Ma, L. Wang and W. Jiang, *Chem. Eng. J.*, 2023, **451**, 139031.
111 H. Jinno, S. B. Shivarudraiah, R. Asbjorn, G. Vagli, T. Marcato, F. T. Eickemeyer, L. Pfeifer, T. Yokota, T. Someya and C. J. Shih, *Adv. Mater.*, 2023, 2304604, DOI: **10.1002/adma.202304604**.
112 J. W. Schall, A. Glaws, N. Y. Doumon, T. J. Silverman, M. Owen-Bellini, K. Terwilliger, M. A. Uddin, P. Rana, J. J. Berry, J. Huang, L. T. Schelhas and D. B. Kern, *Solar RRL*, 2023, **7**, 2300229.
113 W. Nie and H. Tsai, *J. Mater. Chem. A*, 2022, **10**, 19518–19533.
114 S.-H. Chin, L. Mardegan, F. Palazon, M. Sessolo and H. J. Bolink, *ACS Photonics*, 2022, **9**, 2483–2488.
115 S. Yu, J. Hu, H. Zhang, G. Zhao, B. Li, Y. Xia and Y. Chen, *ACS Photonics*, 2022, **9**, 1852–1874.
116 J. Dong, F. Lu, D. Han, J. Wang, Z. Zang, L. Kong, Y. Zhang, X. Ma, J. Zhou, H. Ji, X. Yang and N. Wang, *Angew. Chem., Int. Ed.*, 2022, **61**, 202210322.
117 W. Jiang, S. Lee, G. Zan, K. Zhao and C. Park, *Adv. Mater.*, 2023, 2304053, DOI: **10.1002/adma.202304053**.
118 P. Mao, X. Shan, H. Li, M. Davis, Q. Pei and Z. Yu, *ACS Appl. Electron. Mater.*, 2022, **4**, 568–575.
119 Q. Chang, X. Zhou, S. Jiang, G. Xiang, L. Li, Y. Li, C. Jing, F. Ling, Y. Wang and P. Xiao, *Ceram. Int.*, 2022, **48**, 33645–33652.
120 A. Kirakosyan, M. R. Sihn, M.-G. Jeon, R. M. D. Kabir and J. Choi, *Appl. Mater. Today*, 2022, **26**, 101307.
121 W. Jiang, Z. Zhuo, X. Zhang, H. Luo, L. He, Y. Yang, Y. Wen, Z. Huang and P. Wang, *Food Chem.*, 2024, **431**, 137165.
122 X. He, W. Ji, S. Xing, Z. Feng, H. Li, S. Lu, K. Du and X. Li, *Talanta*, 2024, **268**, 125283.
123 T. Liu, J. He, Z. Lu, M. Sun, M. Wu, X. Wang, Y. Jiang, P. Zou, H. Rao and Y. Wang, *Chem. Eng. J.*, 2022, **429**, 132462.
124 A. Marunchenko, V. Kondratiev, A. Pushkarev, S. Khubezhov, M. Baranov, A. Nasibulin and S. Makarov, *Laser Photonics Rev.*, 2023, **17**, 2300141.
125 S. B. Bhagyalakshmi, D. Zhang and V. Biju, *J. Phys. Chem. C*, 2022, **126**, 17826–17835.
126 M. Alahbakhshi, A. Mishra, G. Verkhogliadov, E. E. Turner, R. Haroldson, A. C. Adams, Q. Gu, J. J. Rack, J. D. Slinker and A. A. Zakhidov, *Adv. Funct. Mater.*, 2023, **33**, 2214215.
127 K. H. Ngai, X. Sun, Y. Wang, L. Lin, Z. Chen, Q. Wei, M. Li, C. Luan, W. Zhang, J. Xu and M. Long, *Adv. Funct. Mater.*, 2023, **33**, 2211830.
128 Y. J. Yu, C. Zou, W. S. Shen, X. Zheng, Q. S. Tian, Y. J. Yu, C. H. Chen, B. Zhao, Z. K. Wang, D. Di, O. M. Bakr and L. S. Liao, *Angew. Chem., Int. Ed.*, 2023, **62**, e202302005.
129 G. Jin, T. Liu, Y. Li, J. Zhou, D. Zhang, P. Pang, Z. Ye, Z. Xing, G. Xing, J. Chen and D. Ma, *Nanoscale*, 2022, **14**, 919–929.
130 C. Wei, W. Su, J. Li, B. Xu, Q. Shan, Y. Wu, F. Zhang, M. Luo, H. Xiang, Z. Cui and H. Zeng, *Adv. Mater.*, 2022, **34**, 2107798.
131 Y. Sun, L. Ge, L. Dai, C. Cho, J. Ferrer Orri, K. Ji, S. J. Zelewski, Y. Liu, A. J. Mirabelli, Y. Zhang, J. Y. Huang, Y. Wang, K. Gong, M. C. Lai, L. Zhang, D. Yang, J. Lin, E. M. Tennyson, C. Ducati, S. D. Stranks, L. S. Cui and N. C. Greenham, *Nature*, 2023, **615**, 830–835.
132 R. Ahmadi, A. Abnavi, H. Ghanbari, H. Mohandes, M. R. Mohammadzadeh, T. De Silva, A. Hasani, M. Fawzy, F. Kabir and M. M. Adachi, *Nano Energy*, 2022, **98**, 107285.
133 L. Li, G. Wang, Y. Rong, Y. Zhang, J. Huang, Y. Zhang, S. Ge, K. Cui, L. Zhang and J. Yu, *Nano Energy*, 2023, **116**, 108768.
134 Z. Yu, H. Gong, Y. Gao, L. Li, F. Xue, Y. Zeng, M. Li, X. Liu and D. Tang, *Small*, 2022, **18**, 2202564.
135 H. You, S. Li, Y. Fan, X. Guo, Z. Lin, R. Ding, X. Cheng, H. Zhang, T. W. B. Lo, J. Hao, Y. Zhu, H. Y. Tam, D. Lei, C. H. Lam and H. Huang, *Nat. Commun.*, 2022, **13**, 6144.
136 L. Guo, Y. Qi, Z. Yang, L. Zhao, W. Zhang, X. Wang, H. Liu, G. Yan, S. Wang and C. Pan, *Nano Energy*, 2022, **102**, 107714.
137 L. Hua, J. Wang, Y. Liu, W. Guo, Y. Ma, H. Xu, S. Han, J. Luo and Z. Sun, *Adv. Sci.*, 2023, **10**, 2301064.
138 M. Min, Y. Liu, C. Song, D. Zhao, X. Wang, Y. Qiao, R. Feng, W. Hao, P. Tao, W. Shang, J. Wu and T. Deng, *ACS Appl. Mater. Interfaces*, 2018, **10**, 21246–21253.
139 J. Meng, P. Zhang, Q. Liu, P. Ran, S. Xie, J. Wei and X. Li, *Acta Biomater.*, 2023, **162**, 20–31.
140 Z. Yang, X. Li, L. Gao, W. Zhang, X. Wang, H. Liu, S. Wang, C. Pan and L. Guo, *Nano Energy*, 2022, **102**, 107743.
141 B. Padha, S. Verma and S. Arya, *Adv. Mater. Technol.*, 2022, **7**, 2200079.
142 Y. Fu, M. Yuan, Y. Zhao, M. Dong, Y. Guo, K. Wang, C. Jin, J. Feng, Y. Wu and L. Jiang, *Adv. Funct. Mater.*, 2023, **33**, 2214094.
143 F. Liu, K. Liu, S. Rafique, Z. Xu, W. Niu, X. Li, Y. Wang, L. Deng, J. Wang, X. Yue, T. Li, J. Wang, P. Ayala, C. Cong, Y. Qin, A. Yu, N. Chi and Y. Zhan, *Adv. Sci.*, 2023, **10**, 2205879.
144 S. Chen, J. Qi, S. Fan, Z. Qiao, J. C. Yeo and C. T. Lim, *Adv. Healthcare Mater.*, 2021, **10**, 2100116.
145 M. Y. Cho, I. S. Kim, S. H. Kim, C. Park, N. Y. Kim, S. W. Kim, S. Kim and J. M. Oh, *ACS Appl. Mater. Interfaces*, 2021, **13**, 5602–5613.
146 Y. Lu, G. Yang, Y. Shen, H. Yang and K. Xu, *Nanomicro Lett.*, 2022, **14**, 150.

147 Y. Ding, Q. Guo, Y. Geng, Z. Dai, Z. Wang, Z. Chen, Q. Guo, Z. Zheng, Y. Li and E. Zhou, *Nano Today*, 2022, **46**, 101586.
148 Y. Liu, T. Chen, Z. Jin, M. Li, D. Zhang, L. Duan, Z. Zhao and C. Wang, *Nat. Commun.*, 2022, **13**, 1338.
149 H. S. Wu, S. M. Wei, S. W. Chen, H. C. Pan, W. P. Pan, S. M. Huang, M. L. Tsai and P. K. Yang, *Adv. Sci.*, 2022, **9**, e2105974.
150 S. Mondal, S. Maiti, T. Paul, A. Sahoo, S. Bhattacharjee, N. S. Das and K. K. Chattopadhyay, *Appl. Mater. Today*, 2022, **26**, 101385.
151 J. Min, S. Demchyshyn, J. R. Sempionatto, Y. Song, B. Hailegnaw, C. Xu, Y. Yang, S. Solomon, C. Putz, L. E. Lehner, J. F. Schwarz, C. Schwarzinger, M. C. Scharber, E. Shirzaei Sani, M. Kaltenbrunner and W. Gao, *Nat. Electron.*, 2023, **6**, 630–641.
152 C. Li, S. Cong, Z. Tian, Y. Song, L. Yu, C. Lu, Y. Shao, J. Li, G. Zou, M. H. Rümmeli, S. Dou, J. Sun and Z. Liu, *Nano Energy*, 2019, **60**, 247–256.
153 T. Wu, Z. Huang, L. Li, W. Sun, T. Xue, Q. Pan, H. Xie, S. Chen, L. Guo, J. Chi, H. Wang, Z. Zhang, T. Han, M. Su and Y. Song, *Adv. Intell. Syst.*, 2022, **5**, 2200307.
154 L. Chen, M. He, L. Li, S. Yuan, A. Chen, M. Chen, Y. Wang, L. Sun, L. Wei, T. Zhang, Q. Li and Q. Zhang, *Chem. Eng. J.*, 2022, **450**, 138279.
155 D. Feng, P. Huang, Y. Miao, A. Liang, X. Wang, B. Tang, H. Hou, M. Ren, S. Gao, L. Geng and A. Luo, *Sens. Actuators, B*, 2022, **368**, 132121.
156 W. Xuan, Y. Chen, D. Hu, X. Gao and S. Huang, *Sens. Actuators, B*, 2023, **397**, 134622.
157 B. Shi, P. Wang, J. Feng, C. Xue, G. Yang, Q. Liao, M. Zhang, X. Zhang, W. Wen and J. Wu, *Nanomicro Lett.*, 2022, **15**, 3.
158 J. Xu, R. Li, Z. Xu, X. Chen, Y. Li, J. Gou, L. Zhang, N. Bi and L. Jia, *J. Lumin.*, 2023, **257**, 119753.
159 Y. Lv, G. Cen, W. Li, C. Zhao and W. Mai, *Sci. China Mater.*, 2023, **66**, 4704–4710.